Composite Structures 319 (2023) 117144

Contents lists available at ScienceDirect

Composite Structures

journal homepage: www.elsevier.com/locate/compstruct

# Lateral deformation behaviour of structural internal replacement pipe repair systems

Shanika Kiriella [a], Allan Manalo [a], Cam Minh Tri Tien [a], Hamid Ahmadi [a,*], Brad P. Wham [b], Ahmad Salah [a], T. Tafsirojjaman [a], Warna Karunasena [a], Patrick Dixon [b], Thomas D. O'Rourke [c]

[a] Centre for Future Materials (CFM), University of Southern Queensland (UniSQ), Toowoomba, QLD 4350, Australia
[b] Center for Infrastructure, Energy, and Space Testing, University of Colorado Boulder, Boulder, CO 80309, US
[c] School of Civil and Environmental Engineering, Cornell University, Ithaca, NY 14853, US

ARTICLE INFO

*Keywords:*
Structural internal replacement pipe (SIRP)
Gas pipelines
Composites
Traffic loading
Finite element analysis (FEA)
Fibre model analysis (FMA)

ABSTRACT

Structural internal replacement pipe (SIRP) systems are emerging composite technologies for the repair of circumferentially cracked host pipes or pipes with joints subject to lateral deformation caused by the surface loads from vehicular traffic. However, laboratory experiments to investigate the suitability of different SIRP systems in repairing full-scale pipes are a very costly and time-consuming process. This paper investigated numerically the behaviour of SIRP repair systems under lateral deformation using the three-dimensional finite element analysis (FEA). The FEA model was validated from the results of the full-scale experimental test. The effect of the crack width of the host pipe, thickness, and material properties of the SIRP, on the bending behaviour of the pipe repair system, was evaluated. The results of the analyses show that the effect of the thickness and elastic modulus of the SIRP on the lateral deformation behaviour is dependent on the width of the circumferential crack in the host pipe. A simplified analytical model based on Fibre model analysis (FMA) and incorporating an average stress factor for host pipes with a narrow crack width was developed to reliably describe the lateral deformation behaviour of the SIRP systems.

## 1. Introduction

A network of 3.2 million kilometres of utility pipes provides critical natural gas service to approximately 80 million people in the United States [1]. However, corrosion of these pipelines which are primarily comprised of legacy cast iron and bare steel is a serious concern for the industry [2–8]. Due to the highly combustible material contained inside, failure in oil and gas pipelines distributed in urban areas can cause catastrophic damage to people, properties, and infrastructure [9–12]. As a result, these critical distribution systems which are nearing or have already exceeded their expected service life require cost-effective repair techniques to restore their original operating capacity, maintain structural integrity, and extend their safe operational life. Rehabilitation of existing pipeline systems is an ideal solution over replacement due to the limited financial resources of asset owners and government institutions [13–15], as well as the complexity of underground structures, buildings and road congestion [16]. This situation has resulted in the investigation and development of various pipe repair technologies [1] suitable for either open trench or trenchless methods [17,18]. In many countries, such as the United States and Canada, the trenchless approach has become the preferred pipe repair method since it reduces environmental damage and excavation operations, making it more reliable and cost-effective [12,19–21]. In recent years, this repair technology has made significant advancements, utilising structural internal replacement pipe (SIRP) systems made from various materials such as thermoplastics, fibre composites [6], polymers and metals [1]. A few recent studies highlighted that while many trenchless repair and installation technologies have grown recently matured, their applicability to oil and gas pipelines is still quite restricted due to their limited technological flexibility and high installation costs [1,22]. Moreover, design procedures and standards for these types of technologies are also unavailable [22]. Consequently, it is essential to assess the suitability of new and emerging SIRP systems to effectively design and utilise them as internal repair systems for pipeline rehabilitation.

* Corresponding author.
*E-mail addresses:* shanika.kiriella@usq.edu.au (S. Kiriella), allan.manalo@usq.edu.au (A. Manalo), camminhtri.tien@usq.edu.au (C.M.T. Tien), hamid.ahmadi@usq.edu.au (H. Ahmadi), brad.wham@colorado.edu (B.P. Wham), ahmad.salah@usq.edu.au (A. Salah), tafsirojjaman@adelaide.edu.au (T. Tafsirojjaman), karu.karunasena@usq.edu.au (W. Karunasena), padi9036@colorado.edu (P. Dixon), tdo1@cornell.edu (T.D. O'Rourke).

https://doi.org/10.1016/j.compstruct.2023.117144
Received 23 January 2023; Received in revised form 19 April 2023; Accepted 8 May 2023
Available online 12 May 2023

The loading conditions have a substantial impact on the failure modes of the host pipes and the SIRP repair systems. Some of the most common failure mechanisms for the SIRP in a host pipe system include lateral deformation [1,23–28], fatigue failure due to repetitive traffic loading [1,23,29], localized fracture and leakage due to internal pressure [1,30,31] and axial deformation due to thermal stresses [1,23,32,33]. Among these, bending deformation due to surface load is considered to be the worst condition for the host pipes and SIRP system [1,23]. The effects of surface loads experienced by the pipelines are normally caused by vehicular traffic [34]. When wheel loads are located directly above the pipe and moving parallel to the longitudinal axis of a pipeline (Fig. 1), the SIRP system undergoes maximum deformation (relative displacement and rotation) at the weakest discontinuity along the underground pipeline [23,35] such as a complete circumferential fracture/round crack and joints [35]. According to Makar et al [36], circumferential cracking is the most typical failure mode for host pipe with a diameter smaller than 380 mm. These cracks on host pipes might occur because of excessive stress generated by ground deformation during trench construction. When such a crack exists on the host pipe, the SIRP may be vulnerable to stresses, relative displacements and rotations caused by the traffic loading [23,35].

With the development of novel pipeline repair systems, the use of fibre composites as a repair material is continuously growing in the oil and gas industry [6,37–42]. This is due to the inherent advantages of fibre composite repair including lightweight, high tensile strength, flexibility in design, versatility in application, and corrosion resistance [38,39,43–45]. However, available studies on the lateral deformation behaviour of circumferentially cracked pipes with an internal composite repair system are limited [23,35,46–48]. Moreover, no comparable standards or regulations for internal composite pipe repair systems currently exist [1]. Because of this, Jeon et al [23] investigated the performance of circumferentially cracked cast iron (CI) pipes with 4 in (101.6 mm), 6 in (152.4 mm) and 8 in (203.2 mm) diameter and repaired them with a Cured-in-Place Pipe (CIPP) liner subject to traffic loading of 133 kN (30 kips). Additionally, an analytical model was developed to evaluate the maximum relative displacements, rotations and stresses induced on the pipeline at the circumferential crack under the traffic loading. However, in their models, it was conservatively assumed that the liner provides zero stiffness because of its significantly lower elastic modulus (E) compared to the CI host pipe. Stewart et al. [35] studied the lateral deformation behaviour of 6 in (152.4 mm) and 12 in (304.8 mm) diameter CI host pipe repaired with CIPP liners having openings ranging from 0.25 in (6.35) to 0.43 in (10. 922 mm) under a lateral loading of 178 kN (40 kips). This study employed field samples from previously lined CI pipes and found that the crack opening affected the overall behaviour of the repaired pipes. Interestingly, the structural contribution of the repair system was not taken into account in their analysis.

Shou and Chen [47] used three-dimensional (3D) finite element analysis (FEA) to investigate the bending response of buried steel pipe with corroded pipe barrels repaired with CIPP liner (using E of 13 GPa and wall thicknesses of 5 mm and 10 mm) under lateral loading. The study revealed that a repair system can enhance the load-carrying capacity of a damaged pipeline. Allouche et al [46] conducted laboratory experimental three-point bending tests to evaluate the bending behaviour of cast iron pipe that was cut into two halves and linked together with a fibre-reinforced polymer (FRP) CIPP subject to both pressurised and non-pressurised circumstances at the location of the pipe joint. They noted that the FRP liner was able to preserve the structural integrity of the system even after the host pipe failed. There was also no visible evidence of leaking observed. In the absence of internal pressure during the bending test, the liner buckled at the invert. In order to establish a range of material properties and thickness of SIRP repair systems appropriate for natural gas pipelines to avoid such types of failure modes, Tafsirojjaman et al [1] studied the lateral deformation behaviour of these technologies under a design load of 178 kN (40 kips) using linear elastic FEA. In their investigation, a wide range of SIRP materials with E ranging from 1 GPa (145 ksi) to 200 GPa (29,008 ksi) and thicknesses between 3.175 mm (0.125 in.) and 25.4 mm (1 in.) were analysed. This study demonstrated that the lateral deformation behaviour is greatly influenced by the thickness and E of the SIRP. In addition, a system must also have an E and thickness of at least 5 GPa and 12.7 mm (12 in.), respectively, to safely bear a lateral load of 178 kN (40 kips), when the strain is limited to 0.02. A few studies that conducted bending analysis on damaged pipes revealed that defect length influences the overall performance of the pipe. Chegeni et al [36] studied the impact of the length of corrosion defects in the longitudinal and circumferential directions of steel pipe on the ultimate load-carrying capacity using FEA. The results indicated that increasing the length of the defect in longitudinal and circumferential directions reduces the ultimate load-carrying capacity of the pipe by 19% and 40%, respectively. This indicated that an increase in defect length along the circumferential direction of the pipe had a greater negative influence on the bending performance of the pipe than an increase in defect length along the longitudinal direction. Shuai et al [37] investigated numerically the effect of corrosion defect length (along the axial direction) on the buckling of the steel pipe under a four-point bending test. The investigators found that the buckling moment of the pipe is a function of the defect length, where a short defect length will fail in single wrinkle buckling, while a long defect length will exhibit two buckling waves. Similarly, Zheng et al [38] highlighted that the maximum axial strain of the pipeline increases with the increase of corrosion defect width. However, it is important to note that most of these studies have analysed the behaviour of the SIRP system either using single material or a continuous pipe system. In actual situations, however, pipes that need a repair system have existing damage like circumferential cracks or discontinuity, e.g., due to the presence of joints. These discontinuities in the host pipe may affect the performance of the SIRP repair system and require detailed investigation.

The thorough evaluation of the effect of different design parameters of SIRP repair systems under flexural loading from laboratory experiments is a very costly and time-consuming process. In contrast, numerical and analytical models need less time, as well as lower costs, however, require validation from physical tests [49]. Once calibrated

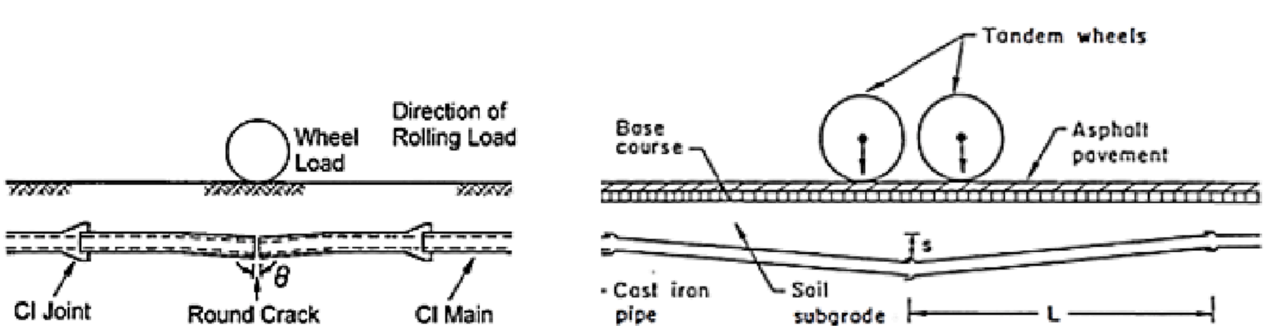


**Fig. 1.** Representation of the deformation of the underground pipeline subjected to traffic loading [35].

and validated from experimental results, numerical and analytical models can be very powerful tools for simulating experimental behaviour and extrapolating them to other conditions. Additionally, numerical and analytical modelling together with experiments, allow a detailed understanding of the actual behaviour of structures which can be used for structural optimization. Therefore, the primary goal of this study is to numerically investigate the performance of SIRP systems for the repair of circumferentially cracked host pipes subject to surface loads and to investigate the effects of important design parameters such as the crack width of the host pipe, thickness and elastic modulus of SIRP on their lateral deformation behaviour. The reliability of the numerical model to evaluate the effect of traffic loads on the SIRP system is validated from the physical four-point bending tests. The findings of this study will provide the research community, product developers and pipeline engineers with a better understanding of the lateral deformation behaviour of circumferentially cracked gas pipelines repaired with SIRP systems.

## 2. Finite element analysis (FEA)

### 2.1. Finite element modelling

A FEA numerical model is created by using ANSYS/Mechanical software [50] to evaluate the behaviour of various SIRP systems including the repair system alone, SIRP in a continuous host pipe (without circumferential crack), and the host pipe with different circumferential crack widths (i.e the host pipe completely fractured into two halves) repaired by a SIRP system under lateral loading. This was accomplished by modelling the experimental four-point bending test at the University of Colorado Boulder with setup dimensions of 762-1016-762 mm (30-40-30 in.), as shown in Fig. 2. This loading configuration represents the wheel loads located directly and moving parallel to the longitudinal axis of a pipeline as reported in [19,31]. A bilinear stress–strain behaviour is used to model the host pipe (Fig. 3a) whereas the SIRP is modelled as a nonlinear material (Fig. 3b). The material properties of ASTM A36 steel host pipe was obtained from [51], whereas that of SIRP was defined by performing tensile tests of the ALTRA10 material in the laboratory in accordance with ASTM D638-10 [52]. The outer diameter and the thickness of the host pipe are 323.85 mm (12.75 in.) and 6.35 mm (0.25 in.) respectively. Based on the inside diameter of the host pipe, the outside diameter of the SIRP is set to 311.15 mm (12.25 in.) and its thickness is 4.1148 mm (0.162 in.). The circumferential crack widths of the host pipe under consideration range from 12.7 to 152.4 mm (0.5 in.–6 in.).

In the parametric study, the effect of different geometrical and material properties such as the repair thickness, crack width of the host pipe, and E of SIRP materials on the lateral deformation of circumferentially cracked host pipes is investigated. Accordingly, SIRP thickness is changed from 3.175 mm (0.125 in.) to 12.7 mm (0.5 in), and the E is varied from 1 GPa (145 ksi) to 200 GPa (29,008 ksi). The SIRP materials that are considered in the parametric study represent polymers, thermoplastics, glass fibre-reinforced polymer (GFRP) composites, and metallic (cast iron and steel) materials. These ranges of thickness and E of the SIRP repair systems are selected based on a previous study by Tafsirojjaman et al. [1]. It was also evaluated whether these systems could provide the structural capacity to withstand a lateral load of 178 kN (40 kips) as suggested by previous studies [1,35,53].

A typical repair scenario in which a steel host pipe having a 50.8 mm (2 in.) circumferential crack repaired by a SIRP material with nonlinear stress–strain behaviour (Fig. 3(b)) and has an elastic modulus and poisons ratio of 3.739 GPa (542.3 ksi) and 0.23 respectively is shown in Fig. 4. For simplification, a quarter model is utilized by applying quarter symmetric boundary conditions in longitudinal and transverse directions. The system is modelled using the standard SOLID186, higher order 3D 20-node solid elements that allow quadratic displacement behaviours and support plasticity, hyper-elasticity, large strain and large deflection capabilities, stress stiffening and creep. The ends of the system are capped by steel blind flanges with properties similar to those of the host pipe. To represent the experimental test setup, pinned supports are used at both ends while the loading head is connected with the pipe clamps via the pin-lug system as shown in Fig. 4. The SIRP repair system is fully bonded to the host pipe. A frictionless connection type is used for the contacts between the host pipe and the supports. Contact pairs include clamp-pipe and lug-pin. Due to the quarter symmetry of the model, only one-fourth of the force is applied to the loading head of the setup vertically in the downward direction. In this study, nonlinear static structural FEA with a full Newton-Raphson solution approach is used to simulate the nonlinearity of both SIRP and host pipe materials. This analysis also allows large deformation and plasticity. The FEA model is validated by comparing numerical results to full-scale experimental data.

### 2.2. Mesh convergence study and mesh refinement

A mesh convergence study is carried out to determine the optimum mesh sizing required for generating reliable and accurate FEA results. This is accomplished by comparing the maximum midspan deflection of the system under lateral loading obtained by FEA with the theoretical results. A single pipe, representing the SIRP, is modelled for this purpose with an E of 200 GPa (29,008 ksi) and subjected to a load of 178 kN (40 kips). The pipe used for mesh convergence analysis has the same

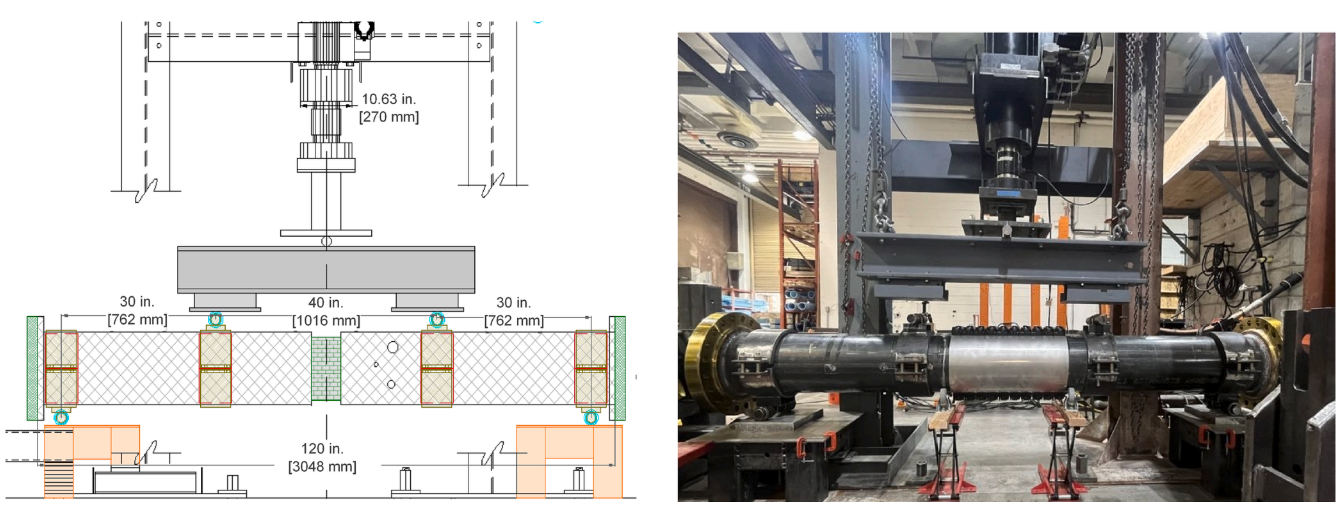


**Fig. 2.** Schematic view (left) and actual set-up (right) for lateral deflection test of SIRP systems (CUB).

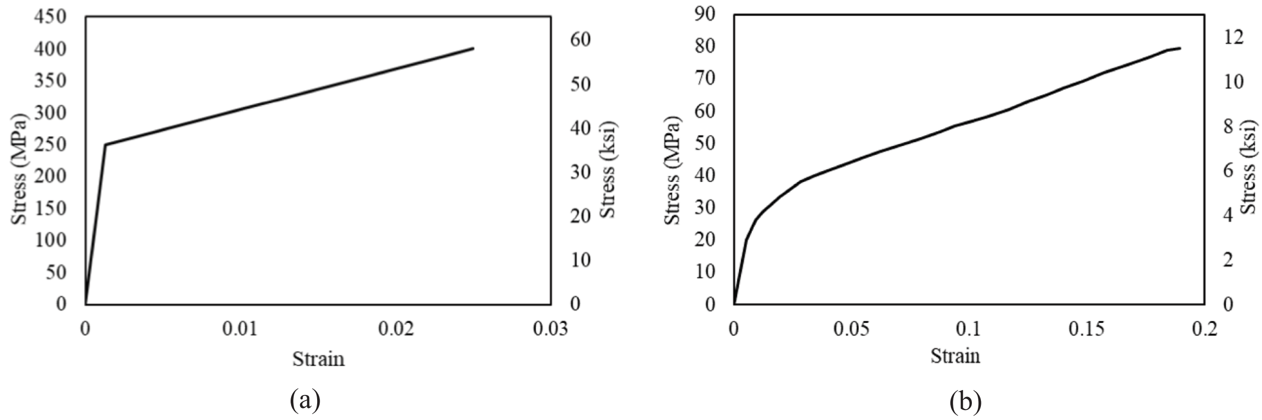


**Fig. 3.** Stress–strain behaviour: (a) Steel host pipe [42], (b) ALTRA10 SIRP.

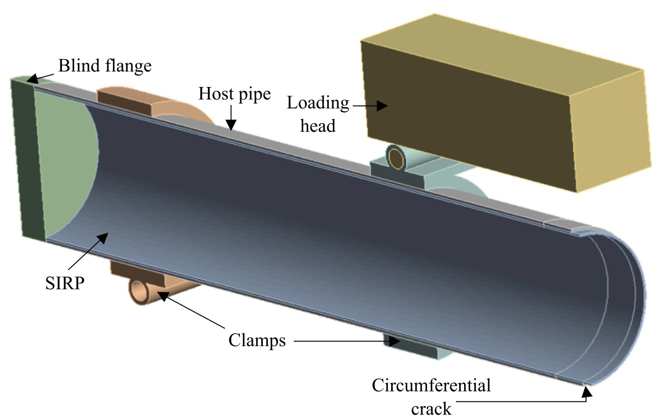


**Fig. 4.** Geometry, boundary conditions and loading of FEA quarter model of SIRP in host pipe with 50.8 mm (2 in.) crack width.

dimensions as the SIRP system described in Section 2.1. In the thickness direction, a mesh size of three elements is utilised, while the surface element sizing is varied from coarse (30 × 30 mm) to very fine (2 × 2 mm). The FEA outcomes are plotted against the total number of elements and compared to the theoretical result of 3.02 mm. According to this mesh convergence study (Fig. 5), as the mesh size decreases, the solutions tend to converge. The solution starts to converge with an accuracy of at least 5.67% when the mesh size is 5 mm or smaller.

A mesh refinement is conducted in order to increase the accuracy of FEA solutions. Refinement is performed by reducing the element size of the mesh in the region of high stresses. Especially a finer mesh is used around the crack edge and midspan. The refined mesh was designed with a surface element size of 2 × 2 mm along the crack and along a distance of 76.2 mm from the crack edge towards the loading point. An optimum surface element size of 5 mm is utilised for the host pipe and SIRP outside the mesh refinement region. Three elements are used in the thickness direction of both the host pipe and the SIRP over their entire lengths.

### 2.3. Validation of FEA model

The FEA model of 4.1148 mm thick SIRP in steel host pipe with 12.7 mm (0.5 in.) crack width is validated in Fig. 6 by comparing it to full-scale laboratory experimental results from the University of Colorado Boulder. The comparison demonstrates that the load–deflection behaviour predicted by the FEA is in good agreement with the experimental outcomes. Under a loading of 14.86 kN (3.34 kips), the maximum discrepancies between the FEA and laboratory experimental deflections at the crack edge (43.35 mm or 1.71 in from midspan) and loading point

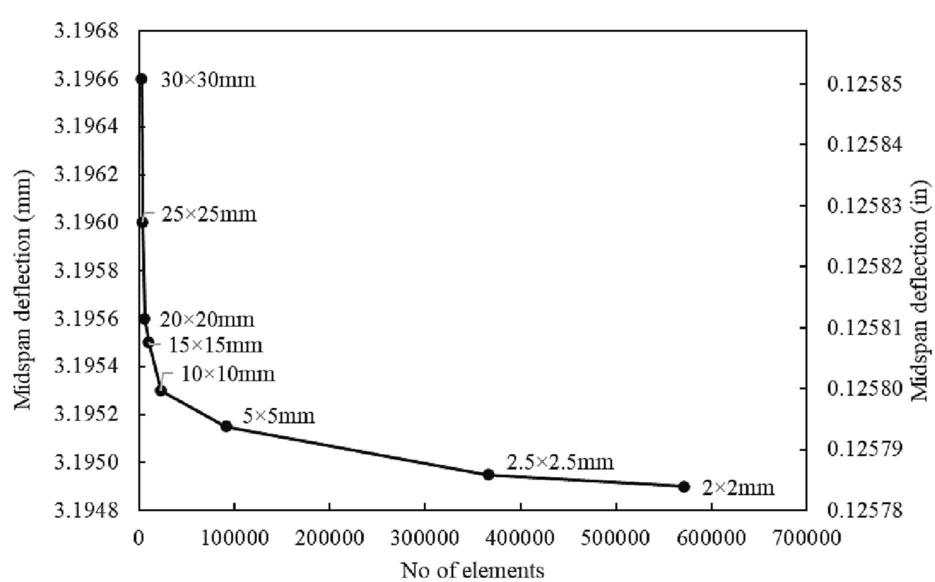


**Fig. 5.** Mesh convergence study.

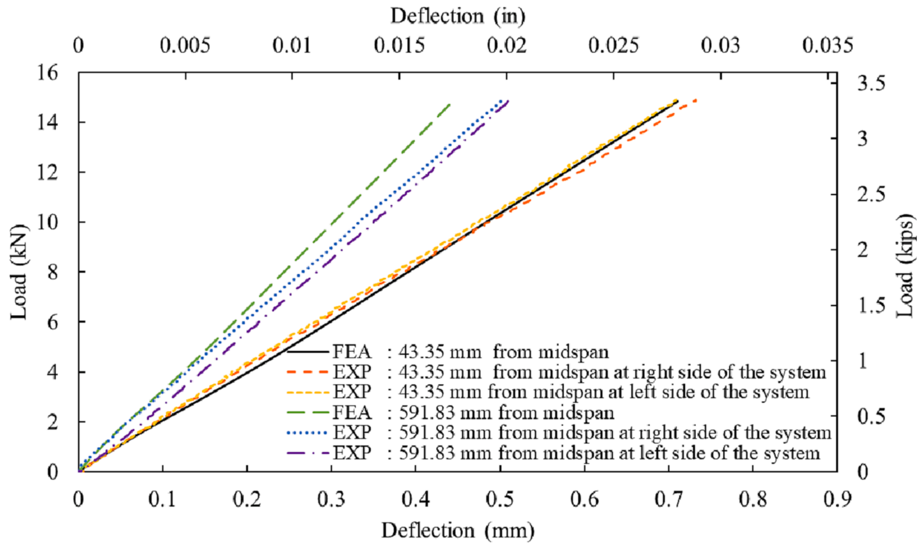


**Fig. 6.** Comparison of FEA and experimental load–displacement behaviours of SIRP in host pipe with 12.7 mm opening.

(591.83 mm or 23.3 in from midspan) are roughly 2.7% and 12.9%, respectively, indicating high accuracy.

## 3. Results and discussions

### 3.1. Behaviour of SIRP repair systems

The nonlinear load-midspan deflection behaviour of a SIRP alone is shown in Fig. 7a. The results showed that the deflection increases linearly with the load up to 18 kN (4.05 kips), after which there is a slight nonlinearity because of the decrease in stiffness until failure at a load of 24.5 kN (5.51 kips). At this level of loading, the compressive strain of SIRP is around 0.8%. This reduction in stiffness is caused by the nonlinearity of SIRP material at higher strain. Fig. 7b illustrates the deflection over the length of SIRP from the left support to the midspan. Due to the quarter symmetry of the FEA model, the deflection along the length of SIRP is only provided for the left-hand side of the model. Under the ultimate load, the deflection along the length of SIRP exhibits a linear relationship up to the loading point followed by a nonlinearly decreasing response up to the midspan. The FEA model shows that compressive buckling of the crown between the loading points governs the failure mechanism of SIRP alone under four-point bending (Fig. 8). This phenomenon is also consistent with the findings in the recent research reported by Tafsirojjaman et al [1] which concluded that SIRP systems with a thickness of 9.5 mm or less are susceptible to compressive buckling.

### 3.2. Behaviour of SIRP repair systems in the continuous steel host pipe

The load-midspan deflection relation of a continuous steel host pipe with the SIRP system is shown in Fig. 9a. The deflection increases linearly with load up to 400 kN (89.9 kips), beyond which there is a significant drop in stiffness due to the yielding of the steel host pipe. At this level of load, it is noted that the SIRP is in the elastic region with a compressive strain of only 0.19%, which is almost 76% lower than that of the SIRP alone. Therefore, it is evident that the host pipe can stabilize the strain that develops in the SIRP at a higher load and prevents buckling failure. The SIRP in a continuous host pipe system fails at a load of 642.3 kN (144.4 kips) owing to buckling of the crown of the combined pipe section at midspan. This investigation reveals that the overall load–deflection behaviour of SIRP in an undamaged host pipe will be highly influenced by the host pipe. Fig. 9a compares the load against the midspan deflection behaviour of the continuous steel host pipe with SIRP to that of a continuous host pipe alone. It can be seen from the figure that the load at the yielding of the continuous host pipe is almost identical to that of the continuous steel host pipe with the SIRP system. This indicates that the presence of the SIRP does not increase the load at the yielding of the host pipe. This is because, up to the yielding point, the

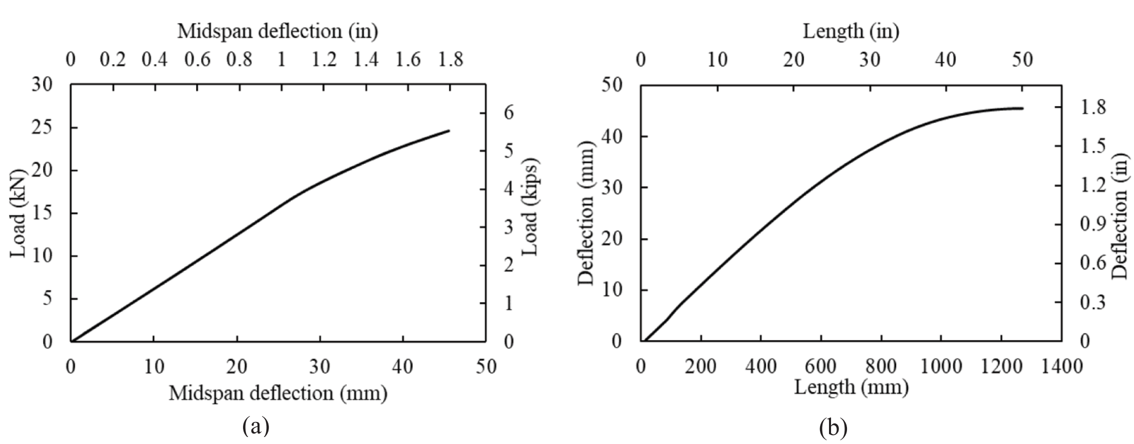


**Fig. 7.** (a) Load vs. maximum deflection behaviour, (b) deflection (at ultimate load) along the half-length (from left support to midspan) of SIRP alone.

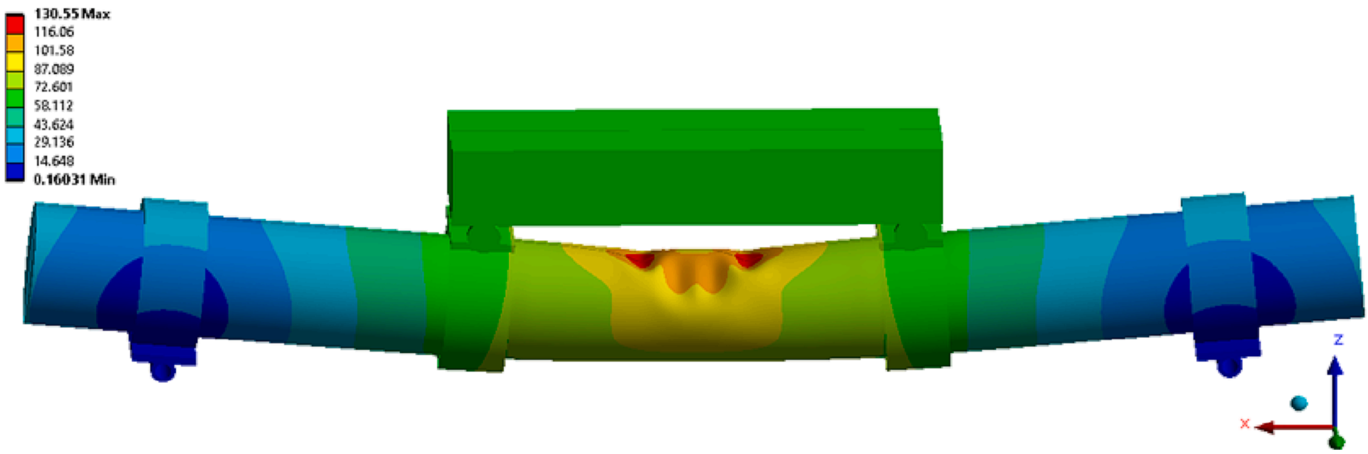


**Fig. 8.** Compressive buckling of the SIRP alone under a four-point bending test.

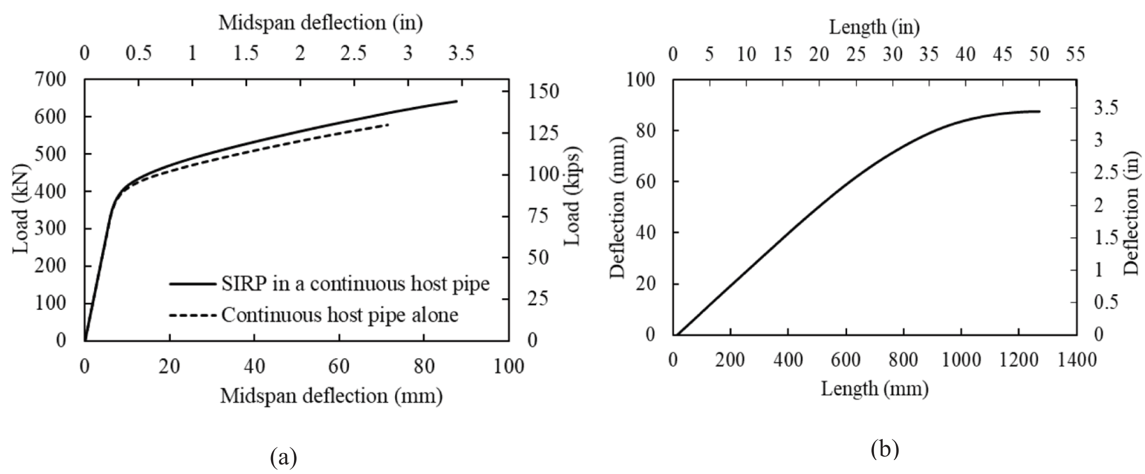


**Fig. 9.** (a) Load vs. maximum deflection behaviours of SIRP in continuous host pipe and continuous host pipe alone (b) deflection (at ultimate load) along the half-length of SIRP in the continuous host pipe.

steel host pipe has a significantly higher modulus of elasticity and stiffness than the SIRP. Thus, with lower modulus and stiffness, the contribution of SIRP to the overall strength of the continuous host pipe system before yielding can be neglected. However, the ultimate load capacity and the maximum midspan deflection of this continuous host pipe alone are respectively around 578.1 kN (130 kips) and 71.35 mm (2.81 in.), which is less than that of the continuous host pipe with SIRP. At the ultimate load of the host pipe alone, the deflection of the host pipe with the SIRP repair system is only 57.19 mm (2.25 in.), which is approximately 20% less than that of the host pipe alone. Furthermore, the failure mechanism of the continuous host pipe alone is local inward buckling of the pipe crown between loading points, which is quite similar to that of SIRP with the continuous host pipe. This indicates that the failure mode of the SIRP-repaired continuous host pipe is controlled by the host pipe. Despite the fact that the host pipe has a greater influence on the load–deflection behaviours than the SIRP, neglecting the mechanical contribution of the thinner SIRP in deflection calculations after the yielding of steel host pipe underestimates the ultimate load-carrying capacity of the system by 11% and its maximum deflection by 23%. Therefore, the frameworks developed in previous studies [23,35] assessing deflection by neglecting the contribution of the repair materials are not applicable to SIRP systems. The deflection along a half-length of the above-mentioned SIRP in a continuous host pipe at its ultimate load, on the other hand, is depicted in Fig. 9b. The figure indicates that at ultimate load, the deflection along the length of the SIRP in the continuous host pipe increases linearly up to the load point, after which it increases nonlinearly and gradually until the midspan.

### 3.3. *Behaviour of SIRP repair systems in host pipe with a circumferential crack*

#### 3.3.1. *Effect of crack width in the host pipe*

The load versus midspan deflection behaviour of a SIRP repair system in a steel host pipe with different crack widths ($l$) under lateral loading is displayed in Fig. 10. The results show a linear load–deflection relationship for crack widths of 12.7 mm (0.5 in.), 25.4 mm (1 in.), 50.8 mm (2 in.), 101.6 mm (4 in.) and 152.4 mm (6 in.), respectively, up to a loading of 23.0 kN (5.17 kips), 20.0 kN (4.5 kips), 16.9 kN (3.8), 16.6 kN (3.73 kips) and 16.1 kN (3.62 kips), followed by a slight nonlinear decrease in stiffness until the systems finally fail at a loading of 83.7 kN (18.82 kips), 61.7 kN (13.87 kips), 35.6 kN (8.0 kips), 29.4 kN (6.61 kips) and 27.9 kN (6.27 kips), respectively. The ultimate failure of these circumferentially cracked host pipes repaired with SIRP systems under bending is governed by outward buckling at the crown of the SIRP (compressive zone) between the crack edges. Fig. 11a, b and c display the compressive buckling of SIRP in host pipe with 50.8 mm (2 in.), 101.6 mm (4 in.) and 152.4 mm (6 in.) crack widths, respectively. A similar failure behaviour was reported in a previous study [46], wherein it was concluded that the absence of internal pressure can cause the liner to buckle during the laboratory experiment of the three-point bending

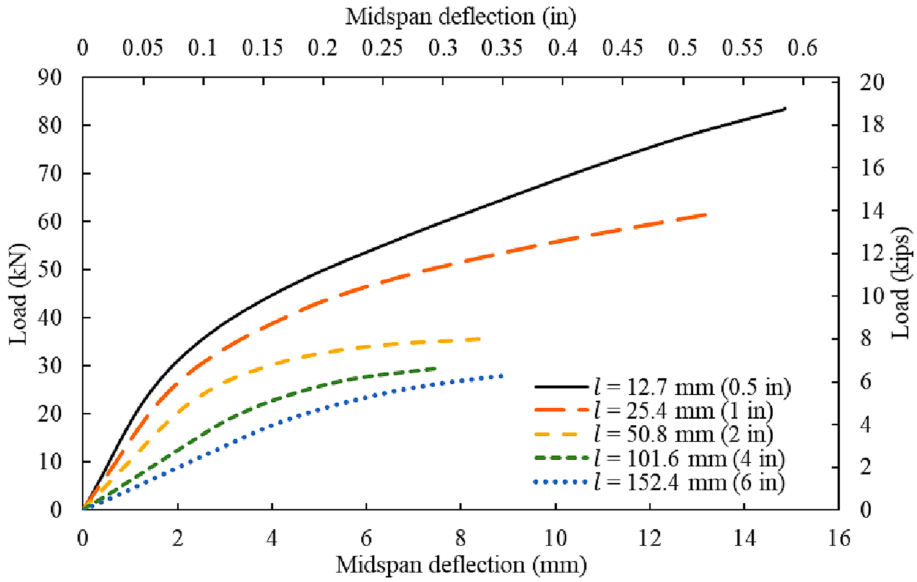


**Fig. 10.** Load- midspan deflection behaviour of SIRP in host pipe with different crack widths.

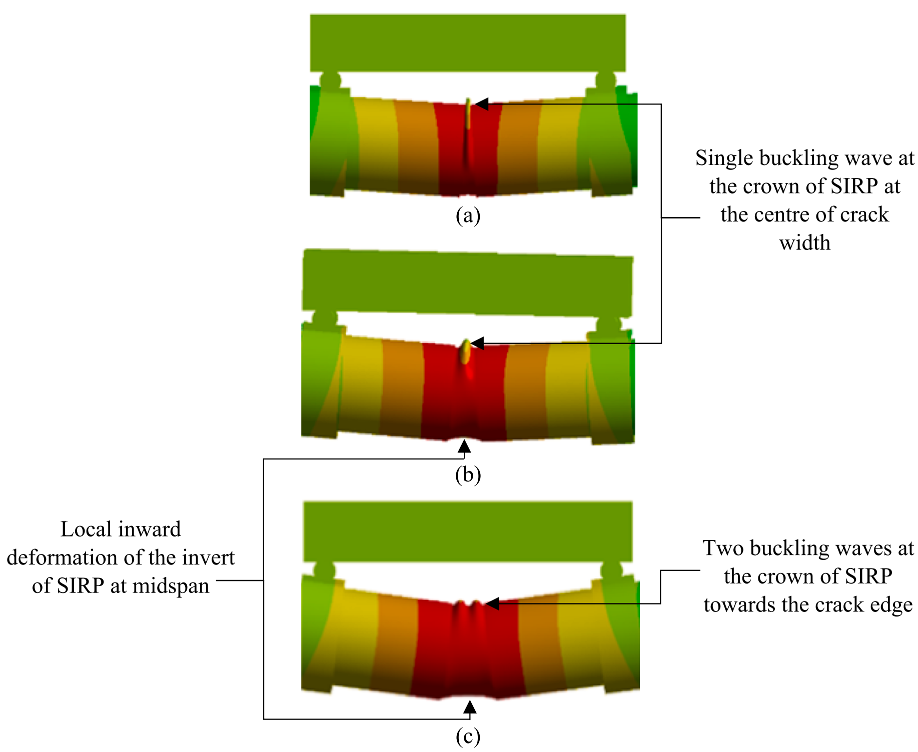


**Fig. 11.** Failure modes of SIRP in a host pipe with wider crack widths, i.e. (a) 50.8, (b) 101.6 mm and (c) 152.4 mm.

test. Fig. 11 shows that only one buckling wave is visible in the middle of the crack width when the width of the opening is 101.4 mm (4 in.) or less, while there are two buckling waves towards the crack edge when the crack width is greater than 101.4 mm (4 in.). These failure behaviours are consistent with the observations of Shuai et al [37]. This failure behaviour indicates that, unlike a continuous host pipe, the failure mechanism of the SIRP in a host pipe with a circumferential crack will be controlled by the SIRP. It is interesting to note that the analysis of the SIRP alone showed similar failure behaviour. However, the buckling load in which the SIRP system failed is higher for narrow crack width, but it converges to the level of the buckling load of SIRP alone with a significantly lower midspan deflection due to the relatively high stiffness of the host pipe.

The influence of crack widths on the ultimate load-carrying capacity of the above-mentioned circumferentially cracked host pipe repaired with SIRP is illustrated in Fig. 12a. It is clear from the results that the lateral load-carrying capacity of SIRP in host pipe systems with very narrow crack widths is considerably higher than those with wide crack widths. When the crack width increases from 12.7 mm (0.5 in.) to about 50.8 mm (2 in.), the ultimate load capacity of the system exhibits a dramatic nonlinear reduction, after which it shows a slight linear decline until the crack widens to 152.4 mm (6 in.). This behaviour may be

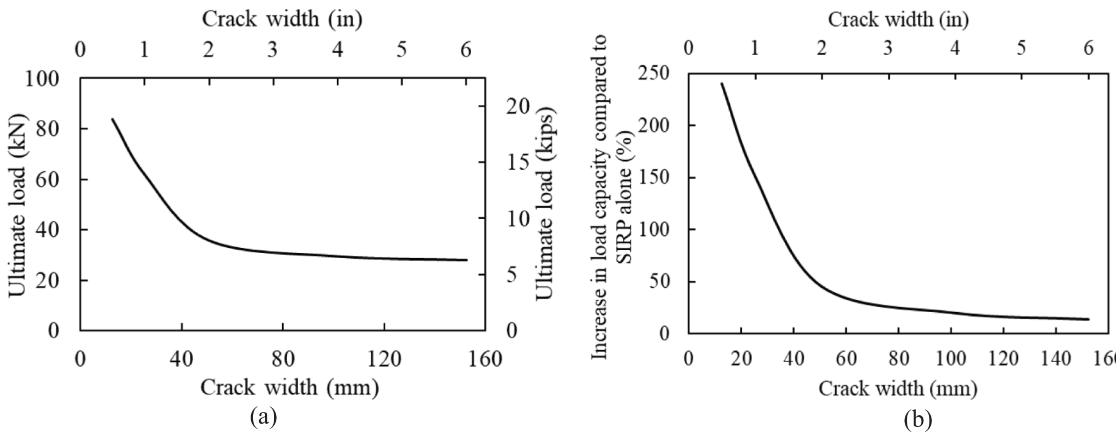


**Fig. 12.** (a) Effect of crack width of host pipe on the ultimate load capacity of ALTRA10 SIRP system (b) Percentage increase in load capacity compared to SIRP alone.

caused by the considerable reduction in the contribution of the host pipe to the overall strength of the SIRP system when the crack widens from 12.7 mm (0.5 in.) to 50.8 mm (2 in.). The overall decrease in ultimate lateral load capacity is approximately 66.7%. Furthermore, none of these SIRP repair systems with 4.1148 mm thickness can provide structural capacity to circumferentially cracked host pipes to safely carry a design load of 178 kN (40 kips). The increase in lateral load capacity relative to SIRP alone for these repair systems with varying crack widths is shown in Fig. 12b as a percentage. It is seen from the graph that the load capacity of the SIRP in a host pipe with a 12.7 mm (0.5 in.) crack width is about 240% higher than that of SIRP alone. On the other hand, the load capacity of the SIRP system with 152.4 mm (6 in.) crack width is only 13.4% greater than that of SIRP alone. As a result, unlike SIRP systems with very narrow crack widths, the ultimate load-carrying capacity of those with wider crack widths is primarily controlled by the SIRP. Additionally, when the crack width is 152.4 mm (6 in.) or longer, the ultimate loading capacity of the SIRP with the host pipe will approach that of the SIRP alone.

The effect of crack width on midspan deformations of the SIRP system (at invert) under loading of nearly 27.9 kN (ultimate loading of the system with 6 in crack width) is shown in Fig. 13. The results reveal that under the same loading level, the SIRP repair system exhibits a slight nonlinear increase in deflection from 12.7 mm (0.5 in.) to 50.8 mm (2 in.) crack widths followed by an almost a linear increment until 152.4 mm (6 in.) crack width. Overall, when the crack width widens from 12.7 mm (0.5 in.) to 152.4 mm (6 in.), the midspan deflection increases by 415.5%. This is because, unlike the SIRP systems with wider crack widths, the overall load–deflection behaviour of those with narrow crack widths is mostly governed by the host pipe, which has almost 53.5 times higher stiffness than SIRP alone and hence results in significantly lower deformations at the same loading. Fig. 14 displays the deflection behaviour of a host pipe with varying crack widths, obtained from the left support to the midspan under loading of 27.9 kN (6.27 kips). Accordingly, the deflection of SIRP increases linearly from support to crack edge for all crack widths. However, from crack edge to midspan, deflection of the systems with 12.7 mm (0.5 in.) and 25.4 mm (1 in.) crack widths rises nonlinearly, whereas those of the systems with 50.8 mm (2 in.), 101.6 mm (4 in.), and 152.4 (6 in.) crack widths decline nonlinearly. This behaviour of SIRP with narrow crack width is related to the high stresses that develop over the crack width as a result of stress concentration at the crack edge. The nonlinear reduction in deflection of SIRP with wider crack widths from crack edge to midspan, on the other hand, is caused by a slight local inward deformation of the SIRP at the midspan at invert (Fig. 11b and c).

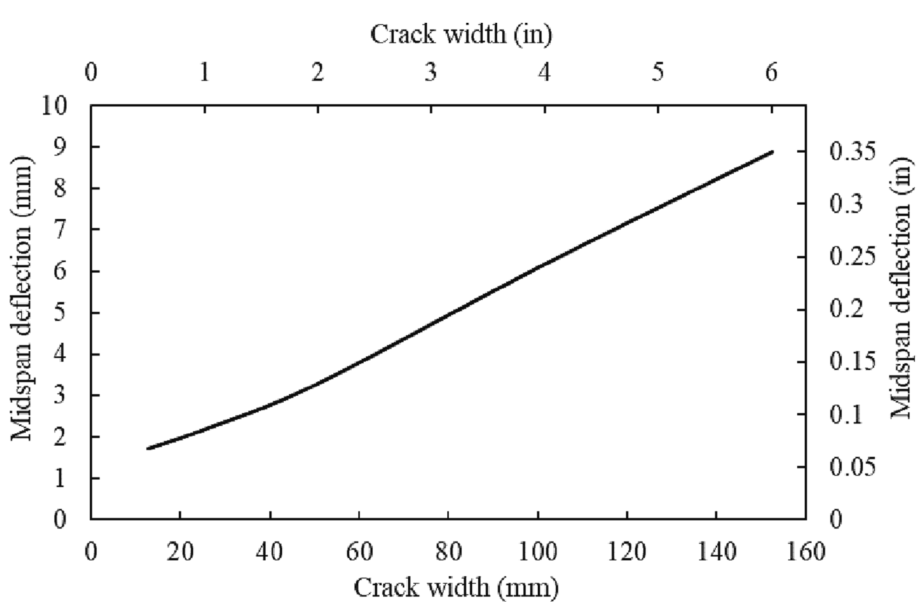


**Fig. 13.** Effect of crack width of host pipe on midspan deflection of SIRP system.

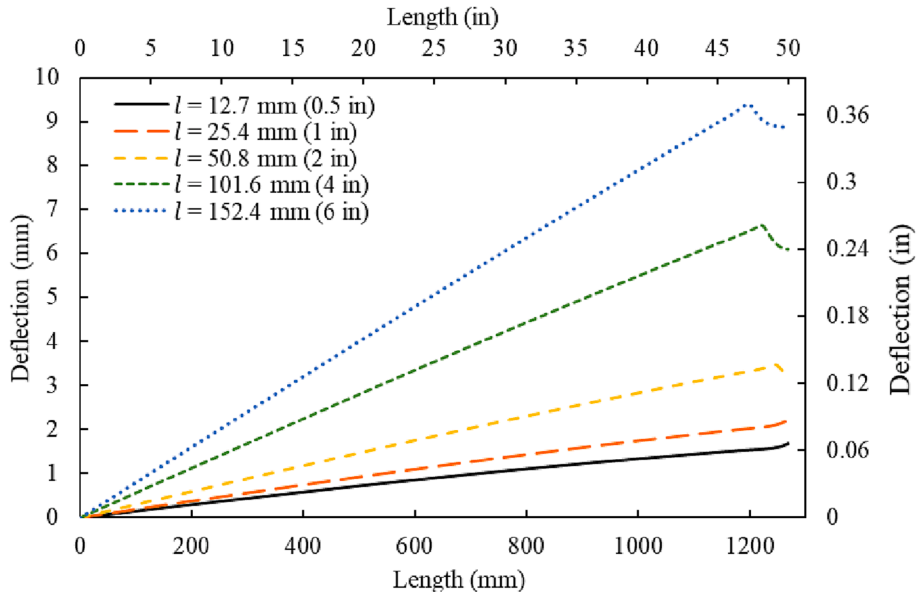


**Fig. 14.** Deflection along the half-length of SIRP in host pipe with different crack widths.

### 3.3.2. *Effect of the thickness of the SIRP system*

Fig. 15 demonstrates how the thickness of the SIRP affects the ultimate lateral load-carrying capacity of the repaired steel pipe with a narrow (12.7 mm) and a wide (152.4 mm) circumferential crack. The results show that when SIRP thickness is increased from 3.175 mm (0.125 in.) to 12.7 mm (0.5 in.), the ultimate load capacity of the system with the wide crack width increases nonlinearly with an overall increment of 773.9% while that of the system with the narrow crack width increases almost linearly with an overall increment of 257.8%. This is because increasing SIRP thickness causes the outer diameter to thickness ratio of SIRP to reduce, making the system less prone to local buckling. The results also reveal that the SIRP system with a narrow crack width requires a repair thickness of at least 9.345 mm (0.368 in.) to be able to safely carry the design load of 178 kN (40 kips). In contrast, even with a maximum thickness of 12.7 mm, the SIRP system with a wider crack width is unable to withstand the design load requirement. Extrapolating the data in Fig. 15, it is evident that the SIRP repair thickness for steel host pipe with a 152.4 mm (6 in.) crack width must be at least 13.854 mm (0.545 in.) to resist the design load. Fig. 16 depicts the influence of the repair thickness on midspan deflection of SIRP in host pipe with varying crack widths under a loading of about 18.08 kN (4.06 kips) (ultimate loading of the SIRP system with 6 in crack width and 3.175 mm repair thickness). According to that, the level of midspan deformation of SIRP systems with 12.7 mm (0.5 in.), 25.4 mm (1 in.), 50.8 mm (2 in.), 101.6 mm (4 in.), and 152.4 mm (6 in.) crack widths appears to decrease nonlinearly by 36.9%, 44.3%, 53.6%, and 63.7%, respectively, as the repair thickness increases from 3.175 mm (0.125 in.) to 12.7 mm (0.5 in.). The reduction in midspan deflection is attributed to the rise in stiffness of the SIRP. Among all crack widths, the SIRP system with the widest opening (152.4 mm or 6 in.) has the highest overall drop in midspan deflection, while the narrowest crack (12.7 mm or 0.5 in.) has the least. This is because the lower flexural stiffness of the SIRP than the host pipe has a greater impact on systems with wide crack widths compared to those with narrow crack widths.

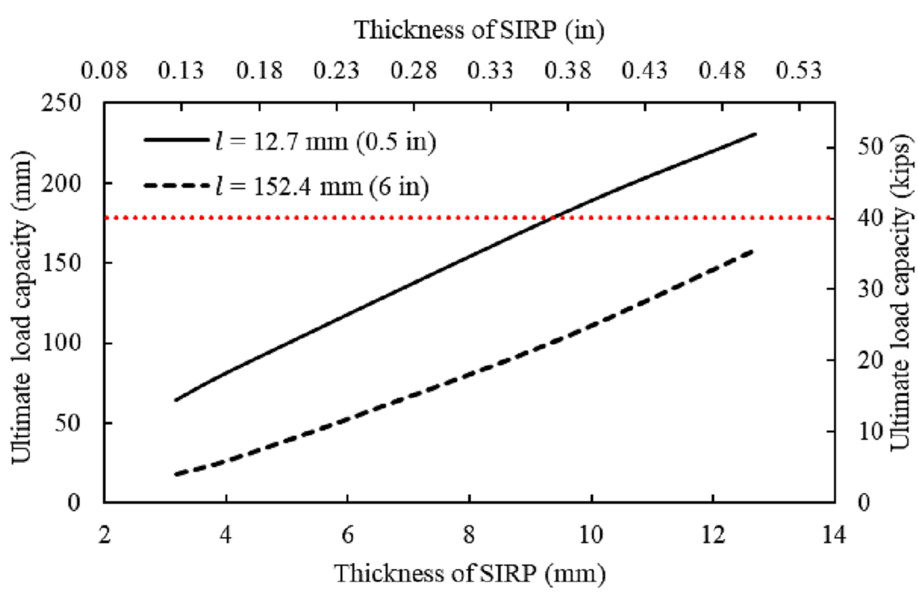


**Fig. 15.** Effect of SIRP thickness on the ultimate load capacity of the pipelines with 12.7 mm (0.5 in.) and 152.4 mm (6 in.) crack widths.

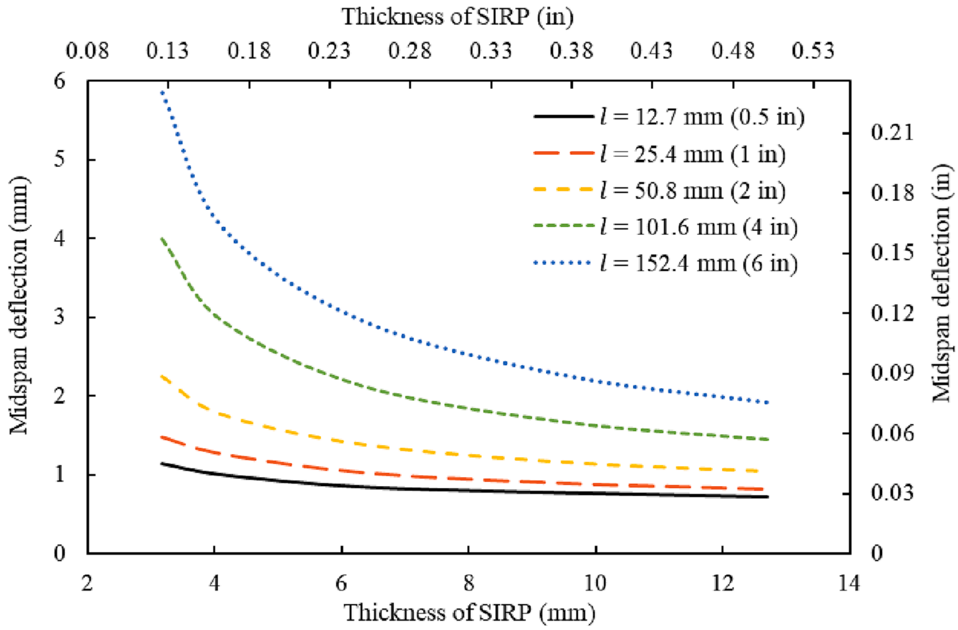


**Fig. 16.** Effect of repair thickness on midspan deflection for different crack widths at a loading of 18.08 kN.

### 3.3.3. Effect of the elastic modulus of the SIRP system

The load–strain behaviour of SIRP material systems with different elastic modulus and with 152.4 mm (6 in.) crack widths at 0.002 and 0.02 strain limitations at the midspan, respectively, is summarised in Fig. 17. The analysis is performed with the same repair thickness of 4.1148 mm (0.162 in.). The load capacities of SIRP made from polymeric materials (1–2 GPa), thermoplastics (3 GPa) and GFRP composites (5–24.5) are investigated at an elastic strain of 0.02, while those of metallic systems including CI (70 GPa) and steel (200 GPa) is evaluated at 0.002 strain. These strain constraints followed the approach implemented by Tafsirojjaman et al [1] that divides the design strain of SIRP materials systems into two categories: 0.02 for composites, polymers, and thermoplastic systems, and 0.002 for metallic systems. It is observed that the load capacity of the SIRP repair system with an E of 24.5 GPa (3,553ksi) or lower is controlled by the compressive buckling at the midspan. The results show that the compressive strain in the SIRP system with an E of 1.744 GPa (252.9 ksi) does not reach the design strain of 0.02 due to geometric nonlinearity at the crown of the SIRP between the crack edges. SIRP materials with E ranging from 2 GPa (290 ksi) to 24.5 GPa (3,553 ksi), on the other hand, approach the design strain of 0.02, exhibiting a nonlinear behaviour at higher strains. Fig. 18 displays the load capacity against E of the SIRP systems. Accordingly, the SIRP system with 152.4 mm (6 in.) crack width and 4.1148 mm (0.162 in.) repair thickness should have an E of at least 13.28 GPa (1,926 ksi) to safely carry the design load of 178 kN. (40 kips).

Fig. 19 illustrates the effect of the *E* of SIRP on the midspan deformation of systems with varying crack widths at the same SIRP thickness under a loading of 13.536 kN (3.043 kips) which is the ultimate load capacity of the SIRP system with 152.4 mm (6 in.) crack and *E* of 1 GPa (145 ksi). The results demonstrate that under the same loading when the

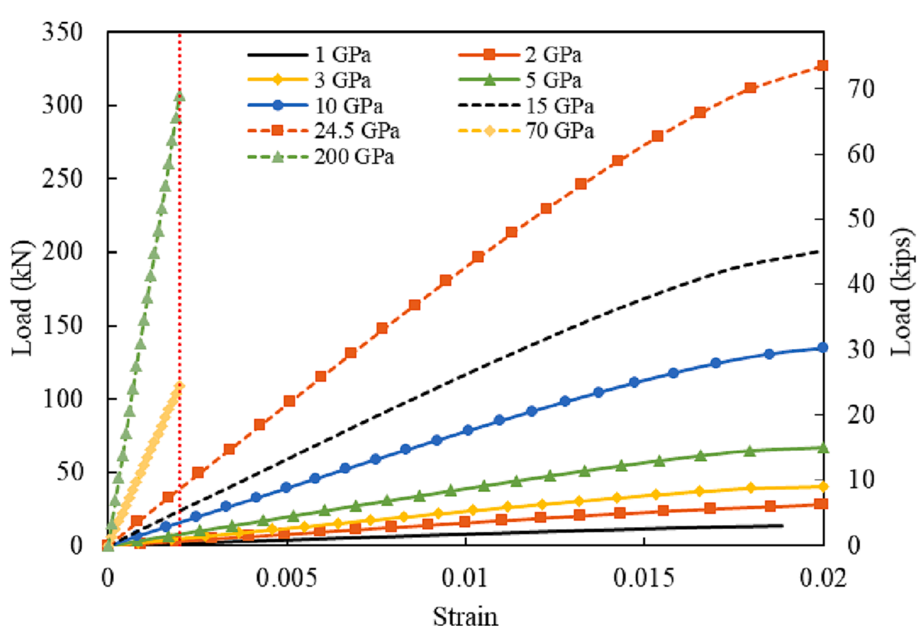


**Fig. 17.** The load-compressive strain behaviour of SIRP systems with 152.4 mm (6 in.) wide cracks repaired using different materials.

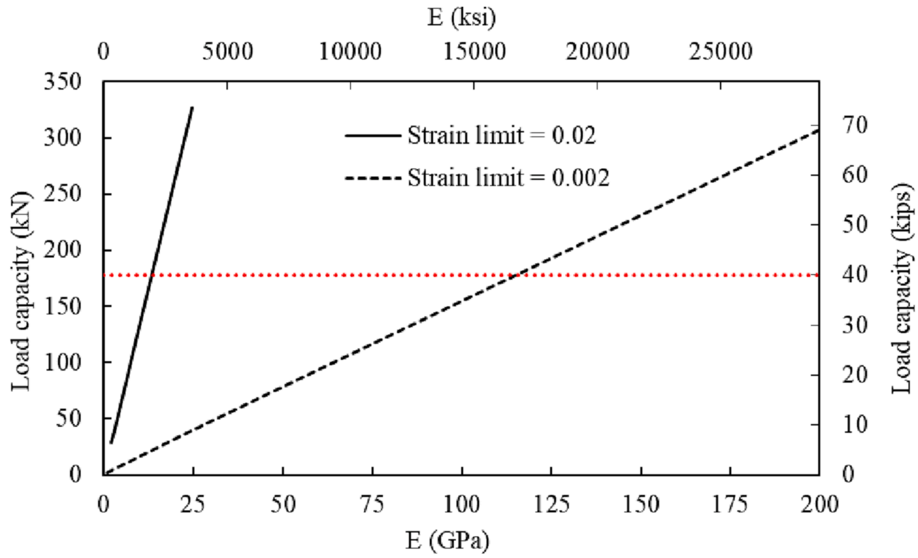


**Fig. 18.** Effect of the E of SIRP on the ultimate load capacity of host pipe with 152.4 mm (6 in.) crack width.

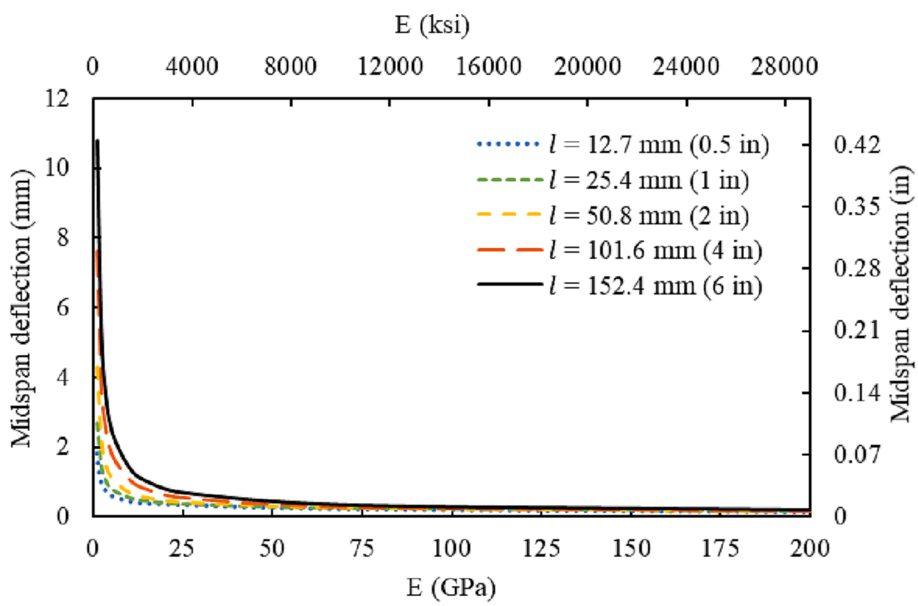


**Fig. 19.** Effect of E of SIRP on midspan deflection for different crack widths.

*E* of SIRP increases from 1 GPa (145 ksi) to 24.5 GPa (3,553 ksi), the midspan deflection drops dramatically in all systems, followed by a slight decrease until the *E* reaches 200 GPa (29,008 ksi). As a result, it is obvious that under the same load levels, the SIRP systems with different stiffnesses in circumferentially cracked host pipes experience different levels of midspan deflection, and the mechanical contribution of the internal replacement pipe is an important aspect in the analysis of SIRP systems. The overall reduction in deflection of the SIRP systems with 12.7 mm (0.5 in.), 25.4 mm (1 in.), 50.8 mm (2 in.), 101.6 mm (4 in.) and 152.4 (6 in.) crack widths, respectively, are 90.6%, 93.6%, 95.9%, 97.6% and 98.2%. Thus, a change in *E* of SIRP has a greater impact on the lateral deformation of the system with wider crack widths than it does with narrower crack widths. The largest difference in deflection (88.1%) between systems with 12.7 mm (0.5 in.) and 152.4 mm (6 in.) occurs when the *E* of the repair material is the lowest, while the least difference (11.4%) arises when the E is the greatest.

## 4. Simplified theoretical prediction of the lateral deformation

While FEA can accurately simulate the bending behaviour of SIRP systems, the process is quite extensive, complex, and requires a longer execution time. This becomes a limitation if material developers in the industry desire to understand how their SIRP system behaves under lateral loading. Thus, the development of a more efficient and simplified analytical model that can still accurately reflect the bending behaviour would be highly beneficial. Considering this requirement, the applicability of the fibre model analysis (FMA) [54] used in the analysis of the layered composite section is investigated to generate simple theoretical predictions of the behaviour of the SIRP system under lateral loading. While this calculation approach can be developed in a Microsoft Excel spreadsheet, the analysis conducted in the current study is implemented using MATLAB [55]. The analysis considers the constitutive nonlinear material behaviour of the host pipe and SIRP as shown in Fig. 3a and b, respectively. In this analysis, it is assumed that the strain in the SIRP and the host pipe is directly proportional to their distance from the neutral axis and that there is a perfect bond between the SIRP and the host pipe. These assumptions are based on the Euler-Bernoulli theorem of strain compatibility, which states that the plain sections remain plane before and after bending which requires perfect bonding between the SIRP and the host pipe materials and no-slip [56]. The fundamental assumptions of FMA are shown in Fig. 20. In the figure, $D_{p(out)}$ is the outer diameter of SIRP, $D_{p(in)}$ is the inner diameter of SIRP, $\sigma_{h(t)}$ and $\varepsilon_{h(t)}$ characterise the tensile strength and tensile strain of the host pipe material, respectively, whereas $\sigma_{h(c)}$ and $\varepsilon_{h(c)}$ represent the compressive strength and corresponding compressive strain of the host pipe. Similarly, $\sigma_{p(t)}$ and $\varepsilon_{p(t)}$ indicate the failure strength and strain of the SIRP material in tension, respectively, while $\sigma_{p(c)}$ and $\varepsilon_{p(c)}$ reflect the compressive strength and corresponding compressive strain of the SIRP material.

Due to the nonlinearity of the materials, when the load increases, variations in stiffness (*EI*) within the layers of cross-section and sections along the longitudinal axis of the SIRP system may occur. To account for this behaviour, the varying *EI* values are predicted, and the deflections are calculated as follows: Firstly, a compressive strain value at the topmost layer of the SIRP alone (at the middle crack) is assumed and the corresponding moment capacity and the applied load are calculated. In addition, the corresponding equivalent effective secant stiffness of SIRP ($(EI)_{SIRP}$) is determined by taking the summation of the secant stiffness of all the layers of the SIRP section as shown in Eq. (1). A separate FMA is then performed by increasing the maximum bending strain value at the topmost layer of the host pipe with SIRP section from a lower value to a higher value to determine moment capacities and corresponding equivalent effective secant stiffnesses (Eq.(2)). The moment capacities against the equivalent effective secant stiffness of the cross-section of SIRP with the host pipe ($(EI)_{EFF}$) is then plotted. Thirdly, the loading length of the beam is divided into small segments and the moment capacity at each segment is calculated using the applied load obtained from the previous analysis of the SIRP section alone. The $(EI)_{EFF}$ values corresponding to these moments over the loading length are obtained using $(EI)_{EFF}$ versus moment capacity plot of the host pipe with SIRP section via interpolation curve fit.

$$(EI)_{SIRP} = \sum_{i=1}^{n_{p(c)}} E_{p(c)i} I_{p(c)i} + \sum_{i=1}^{n_{p(t)}} E_{p(t)i} I_{p(t)i} \quad (1)$$

$$(EI)_{EFF} = \sum_{i=1}^{n_{h(c)}} E_{h(c)i} I_{h(c)i} + \sum_{i=1}^{n_{p(c)}} E_{p(c)i} I_{p(c)i} + \sum_{i=1}^{n_{h(t)}} E_{h(t)i} I_{h(t)i} + \sum_{i=1}^{n_{p(t)}} E_{p(t)i} I_{p(t)i} \quad (2)$$

where $E_{h(c)i}$, $E_{p(c)i}$, $E_{h(t)i}$ and $E_{p(t)i}$ are the secant modulus of each layer of host pipe in compression, SIRP in compression, host pipe in tension and SIRP in tension, respectively, while $I_{h(c)i}$, $I_{p(c)i}$, $I_{h(t)i}$ and $I_{p(t)i}$ are the corresponding moment of inertia of each layer of host pipe in compression, SIRP in compression, host pipe in tension and SIRP in tension, respectively.

The maximum midspan deflection of SIRP in a circumferentially cracked host pipe with nonlinear stress–strain behaviour is then determined using Eq. (3). A schematic diagram of SIRP in a host pipe with a middle crack is shown in Fig. 21 where $\Delta_{max}$ is the maximum mid-span deflection, $L$ corresponds to the length of the SIRP between supports, $\frac{(L-l)}{2}$ is the length of one of the cracked host pipe sections, $l$ is the crack width, $P$ is half of the applied load $n$ is the total number of segments into which the loading length, $a$ is subdivided, $w_i$ is the length to the right boundary of each segment from the left support, $(EI)_{eff_i}$ is the equivalent effective secant stiffness of the cross-section of each segment SIRP segment with host pipe over the length $a$ (on the left side of the system) from the support to the loading point. Finally, by increasing the compressive strain value at the mid-span of SIRP alone from a very lower value to a higher value, a series of corresponding applied loads, $(EI)_{SIRP}$ and $(EI)_{EFF}$ values over the length and the corresponding maximum midspan deflection of SIRP in a host pipe with a middle crack with

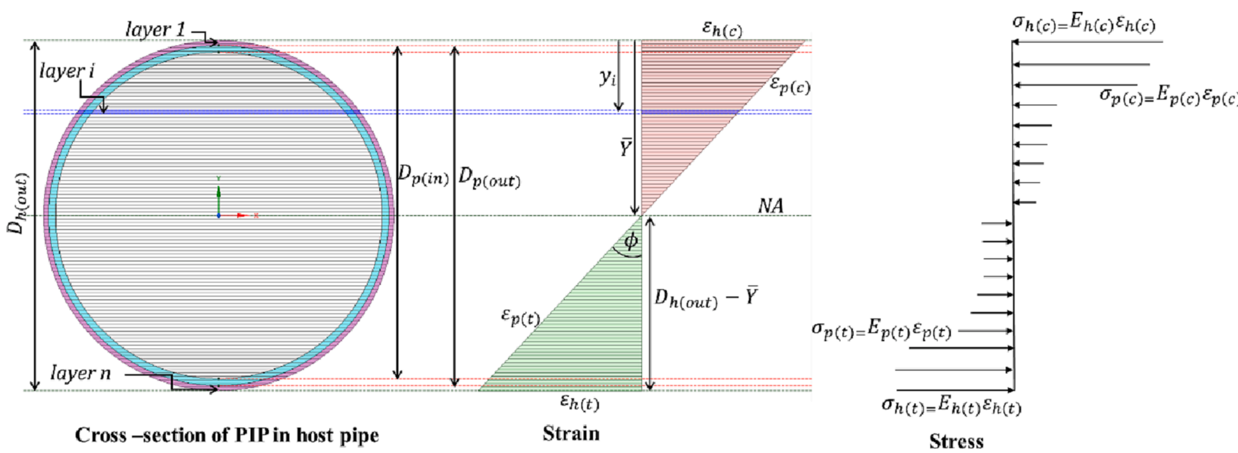


**Fig. 20.** Fundamental assumptions of FMA.

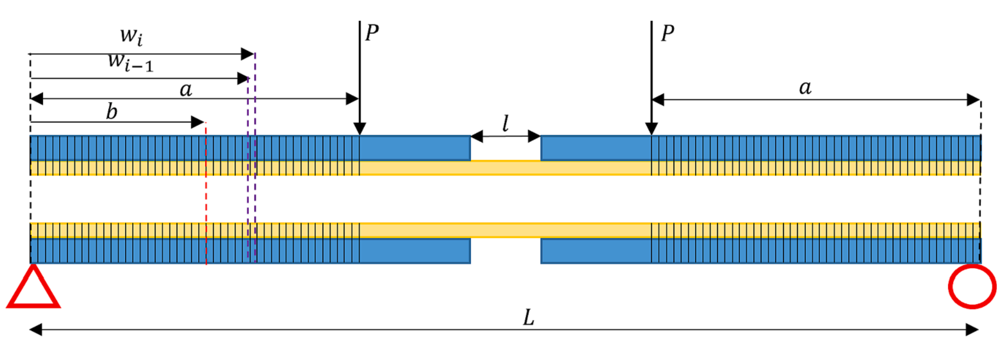


**Fig. 21.** Schematic illustration of SIRP in host pipe with a circumferential middle crack.

nonlinear stress–strain behaviour is computed. The deflection along $0 \le b \le a$, $a \le b \le \frac{(L-l)}{2}$ and $\frac{(L-l)}{2} \le b \le \frac{L}{2}$ of SIRP is predicted using Eqs. (4)–(6) respectively, where $b$ is the length from the left support to the point where the deflection requires to be computed (Fig. 21).

Appropriate place for insertion of Fig. 21

$$\Delta_{\max} = 2\left\{ \sum_{i=1}^{n}\left[\frac{P(w_i^3 - w_{i-1}^3)}{6(EI)_{eff_i}}\right] + \frac{Pa}{16(EI)_{EFF}}\left((L-l)^2 - 4a^2\right) + \frac{Pa}{16(EI)_{SIRP}}\left(2Ll - l^2\right)\right\} \tag{3}$$

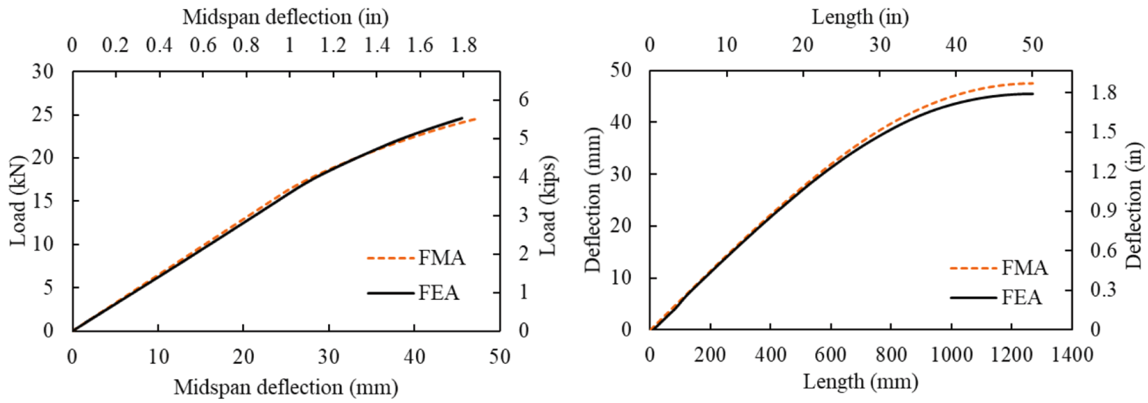


(a) (b)

**Fig. 22.** Comparison of FMA and FEA (a) load- midspan deflection behaviour, (b) deflection (at ultimate load) over the half-length (from left support to midspan) of SIRP alone.

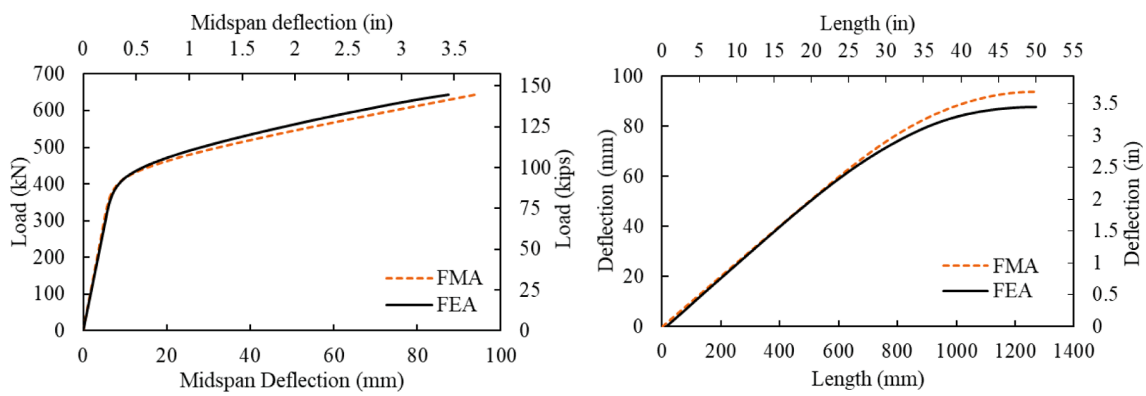


(a) (b)

**Fig. 23.** Comparison of FMA and FEA (a) load- midspan deflection behaviour, (b) deflection (at ultimate load) over the half-length of SIRP in a continuous host pipe.

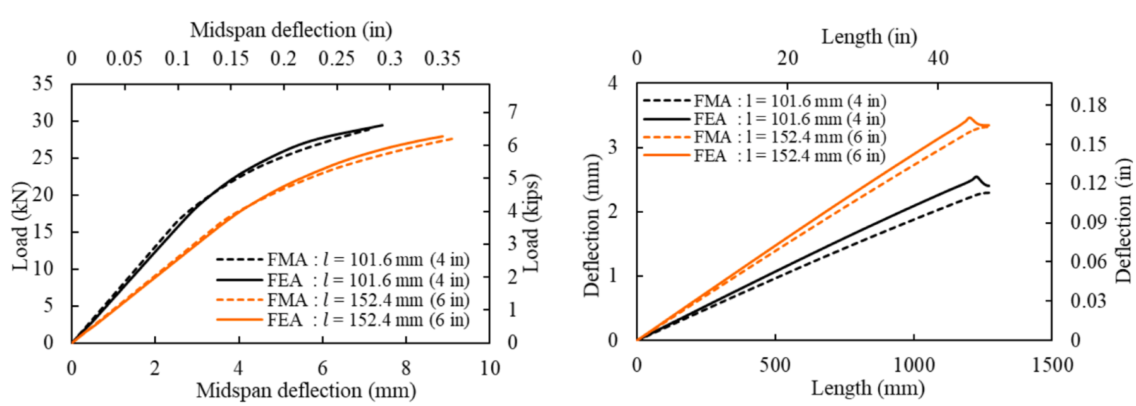


(a) (b)

**Fig. 24.** Comparison of FMA and FEA (a) load- midspan deflection behaviour and (b) deflection along half-length of SIRP in host pipe with wider crack widths.

The deflection at any point along $0 \le b \le a$:

$$\Delta_{(0\le b\le a)} = \sum_{i=1}^{n_b}\left\{\frac{P\left(1-\frac{b}{L}\right)\left(w_i{}^3-w_{i-1}{}^3\right)}{3(EI)_{eff_i}}\right\} + \sum_{i=1}^{(n-n_b)}\left\{\frac{Pb}{(EI)_{eff_{(a-b)_i}}}\left[\left(\frac{w_i{}^2-w_{i-1}{}^2}{2}\right)-\left(\frac{w_i{}^3-w_{i-1}{}^3}{3L}\right)\right]\right\} + \frac{Pab}{(EI)_{EFF}}\left\{\frac{L-l}{2}-a-\frac{(L-l)^2}{8L}+\frac{a^2}{2L}\right\}+\frac{Pabl}{2(EI)_{PIP}} + \frac{Pab}{(EI)_{EFF}}\left\{\left(\frac{L}{2}-a-\frac{l}{2}\right)-\frac{1}{2L}\left[(L-a)^2-\frac{(L+l)^2}{4}\right]\right\} + \sum_{i=1}^{n}\left\{\frac{Pb}{\left((EI)_{eff}\right)'_i}\left[L(w_i-w_{i-1})-\left(w_i{}^2-w_{i-1}{}^2\right)+\frac{1}{3L}\left(w_i{}^3-w_{i-1}{}^3\right)\right]\right\} \tag{4}$$

The deflection at any point along $a \le b \le \frac{(L-l)}{2}$:

$$\Delta_{\left(a\le b\le\frac{L-l}{2}\right)} = \sum_{i=1}^{n}\left\{\frac{P\left(1-\frac{b}{L}\right)\left(w_i{}^3-w_{i-1}{}^3\right)}{3(EI)_{eff_i}}\right\} + \frac{Pa\left(1-\frac{b}{L}\right)\left(b^2-a^2\right)}{2(EI)_{EFF}} + \frac{Pab}{8L(EI)_{EFF}}\left(3L^2-2Ll-8bL-l^2+4b^2\right)+\frac{Pabl}{2(EI)_{SIRP}} + \frac{Pab}{(EI)_{EFF}}\left\{\left(\frac{L}{2}-a-\frac{l}{2}\right)-\frac{1}{2L}\left[(L-a)^2-\frac{(L+l)^2}{4}\right]\right\} + \sum_{i=1}^{n}\left\{\frac{Pb}{\left((EI)_{eff}\right)'_i}\left[L(w_i-w_{i-1})-\left(w_i{}^2-w_{i-1}{}^2\right)+\frac{1}{3L}\left(w_i{}^3-w_{i-1}{}^3\right)\right]\right\} \tag{5}$$

The deflection at any point along $\frac{(L-l)}{2} \le b \le \frac{L}{2}$:

$$\Delta_{\left(\frac{L-l}{2}\le b\le\frac{L}{2}\right)} = \sum_{i=1}^{n}\left\{\frac{P\left(1-\frac{b}{L}\right)\left(w_i{}^3-w_{i-1}{}^3\right)}{3(EI)_{eff_i}}\right\} + \frac{Pa}{8(EI)_{EFF}}\left[(L-l)^2-4a^2\right] + \frac{Pa\left(1-\frac{b}{L}\right)\left[4b^2-(L-l)^2\right]}{8(EI)_{SIRP}} + \frac{Pab\left\{\frac{L+l}{2}-b-\frac{(L+l)^2}{8L}+\frac{b^2}{2L}\right\}}{(EI)_{PIP}} + \frac{Pab}{(EI)_{EFF}}\left\{\left(\frac{L}{2}-a-\frac{l}{2}\right)-\frac{1}{2L}\left[(L-a)^2-\frac{(L+l)^2}{4}\right]\right\} + \sum_{i=1}^{n}\left\{\frac{Pb}{\left((EI)_{eff}\right)'_i}\left[L(w_i-w_{i-1})-\left(w_i{}^2-w_{i-1}{}^2\right)+\frac{1}{3L}\left(w_i{}^3-w_{i-1}{}^3\right)\right]\right\} \tag{6}$$

where $\Delta_{(0\le b\le a)}$, $\Delta_{\left(a\le b\le\frac{L-l}{2}\right)}$ and $\Delta_{\left(\frac{L-l}{2}\le b\le\frac{L}{2}\right)}$ are the deflection at any point along $0 \le b \le a$ , $a \le b \le \frac{(L-l)}{2}$ and $\frac{(L-l)}{2} \le b \le \frac{L}{2}$ of SIRP, respectively, $n_b$ and $(n-n_b)$ are respectively the number of segments over length $b$ and length $(a-b)$-, $(EI)_{eff_{(a-b)_i}}$ is the equivalent effective secant stiffness of the cross-section of each segment of SIRP with host pipe over length $(a-b)$ from length $b$ to the loading point and $\left((EI)_{eff}\right)'_i$ is the equivalent effective secant stiffness of the cross-section of each segment of SIRP with host pipe over the length $a$ (on the right side of the system) from the loading point to support.

### 4.1. Comparison with FEA results

#### 4.1.1. SIRP repair systems only

The load-midspan deflection behaviour and the deflection (at ultimate load) over a half-length of a SIRP alone obtained from FMA and FEA are compared in Fig. 22a and b respectively. Fig. 22a demonstrates that the nonlinear load-midspan deflection response of SIRP predicted by FMA correlates well with FEA, with a maximum discrepancy of only about 4.1%. This minor deviation can be attributed to geometric nonlinearity considered by the FEA due to the local buckling of SIRP at the midspan. FMA, on the other hand, is a simplified approach that does not capture every single change in 3D geometry including local bucking during bending. As shown in Fig. 22b, the FMA deflection prediction along the half length of SIRP at ultimate load exhibits a linear response up to the loading point followed by a nonlinear response. These FMA results are also found to be in close agreement with FEA ones.

#### 4.1.2. SIRP repair systems in a continuous host pipe

A comparison between the FMA and FEA load-midspan deflection relation and the deflection (at ultimate load) along the half-length of a continuous steel host pipe with SIRP is shown in Fig. 23a and b, respectively. The load-midspan deflection response of SIRP in continuous steel host pipe under bending predicted by FMA is very similar to that of FEA, with a maximum deviation in deflection of only about 12.7% at a load of 546 kN, as shown in Fig. 23a. This difference is because, unlike FMA, which only considers material nonlinearity, 3D FEA nonlinear analysis incorporates geometric nonlinearity, which causes the stiffness of the beam to rise when deformations are large. Enabling large deflection ensures that the program accounts for the change in stiffness caused by geometric changes. Since curved beams have a greater stiffness than straight beams, when a straight beam is turned into a curved beam, its stiffness increases, resulting in less vertical downward deflection than FMA at the same loading level. This increase in stiffness is also called stress stiffening. Fig. 23b indicates that the deflection along the length of the SIRP in continuous host pipe at the ultimate load predicted using FMA, which exhibits a linear response up to the loading point followed by a nonlinear response until midspan, correlates well with the FEA behaviour, with the maximum deviation being only 6.6% at midspan.

#### 4.1.3. SIRP repair systems in a host pipe with wide circumferential cracks

The load versus midspan deflection behaviour of SIRP repair systems in host pipe with wide circumferential crack widths predicted by FMA is compared to FEA results in Fig. 24a. The FMA findings for crack widths of 101.6 mm (4 in.) and 152.4 mm (6 in.) show a linear load–deflection relationship up to 16.8 kN (3.78 kips) and 16.6 kN (3.73 kips), respectively. Thereafter, a slightly nonlinear decrease in stiffness occurs until it finally fails at loadings of 29.4 kN (6.61 kips) and 27.9 kN (6.27 kips), respectively. This overall behaviour of FMA is in good agreement with FEA, with a maximum deviation of less than 6%. Fig. 24b compares the FMA and FEA predictions of deflection along the half-length of the SIRP systems under a load of 15 kN (3.37 kips). Accordingly, it is confirmed that FMA can capture a linear deflection response along the pipe length up to the crack edge, which is similar to the behaviour predicted by FEA. However, the deviation of the FMA prediction from the FEA results rises gradually from the support to the crack edge, and it can be as high as 9.3% at the crack edge of the SIRP system with a crack width of 101.6 mm (4 in.), which is more than twice that at the midspan under the same load. The difference between FMA and FEA prediction is that when the crack width narrows, stress concentration at the crack edge causes an increase in stresses along the crack width in 3D FEA models. This results in higher average stress over the narrow crack width, which the simplified FMA model cannot account for. However, for crack widths narrower than 101.6 mm (4 in.), the average stress along them further increases, resulting in considerable differences between the initial FMA and FEA deflection predictions. To overcome this limitation of the initial FMA, a factor termed the average stress factor ($K$) is established and incorporated into the simplified FMA models to be applied in the deflection computation of SIRP systems with narrow crack widths.

### 4.2. Average stress factor

The average stress factor ($K$) is computed by dividing the average of FEA normal stress along the crack width (at the invert of SIRP) by the corresponding average FMA stresses. The initial FMA deflection prediction is then multiplied by $K$, to obtain the factored FMA deflection, which accounts for the effect of stress concentration on average stresses over crack width. Then, a parametric study is carried out using both FMA and FEA to produce an equation that can accurately estimate the average stress factor. For this, a range of SIRP thicknesses between 3.175 mm (0.125 in.) and 9.525 mm (0.375 in.), crack widths from 12.7 mm (0.5 in.) to 152.4 mm (6 in.) and elastic moduli of materials from 1 GPa (145 ksi) to 200 GPa (29008 ksi) are considered. The parametric analysis shows that the average stress factor is mostly governed by the geometry of the fracture, i.e. the width of the crack and the thickness of SIRP, whereas the E of the material has almost no effect. This is because, under the same load, the stress is determined primarily by the applied load and geometry and does not depend on the E in the elastic region. Fig. 25a compares the effect of crack width on the average stress factor of a repaired host pipe with varied SIRP thicknesses. Accordingly, the average stress factor for a given SIRP thickness reduces with increasing crack width and reaches a constant value once the crack width exceeds 101.6 mm (4 in.). This is due to the fact that when the crack width widens, the local stresses produced by the host pipe discontinuities stabilise along the crack width, resulting in a reduction in average stress. In contrast, when the crack width narrows, the average stress factor increases dramatically. This is because the crack width is insufficient to stabilise the higher stresses leading to an increase in average FEA stress over it. The influence of relative SIRP thickness on the average stress factor of SIRP in host pipes with varied crack widths is shown in Fig. 25. For a given crack width, the average stress factor rises linearly as the relative SIRP thickness increases.

By considering the $K$ as a function of two governing dimensionless parameters, crack width to the thickness of SIRP and the total wall thicknesses of SIRP and host pipe thickness to the thickness of SIRP, a mathematical formulation (Eq. (7)) is developed. This was performed by nonlinear-least squares regression analysis in MATLAB to achieve the best surface fit (Fig. 26). The model equation used in this analysis is Eq. (8), where $t_T$ is the total wall thickness, $t_p$ is the thickness of SIRP, $p$, $q$, $r$ and $s$ are the unknown parameters, and $x$ and $y$ are the total wall thicknesses to SIRP thickness and crack widths to SIRP wall thickness, respectively.

$$K = 1.097e^{-0.01529\left(\frac{t_T}{t_p}\right)} + 1.461e^{-0.3368\left(\frac{l}{t_p}\right)} \tag{7}$$

$$K = pe^{q(x)} + re^{-s(y)} \tag{8}$$

### 4.3. Factored FMA for deflection prediction of SIRP systems with narrow crack widths

The factored FMA deflection of a very narrow crack width (12.7 mm) is compared to both FEA and full-scale laboratory experimental results from the University of Colorado Boulder in Fig. 27. The comparison demonstrates that the load–deflection behaviour predicted by the factored FMA for SIRP with narrow crack widths is in good agreement with the FEA and experimental outcomes. At a loading of 14.9 kN (3.35 kips), the differences between factored FMA and FEA deflection

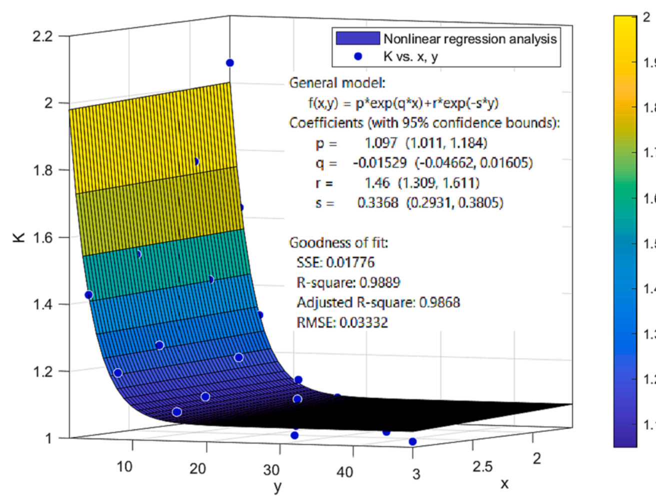


**Fig. 26.** 3D surface fitting in MATLAB.

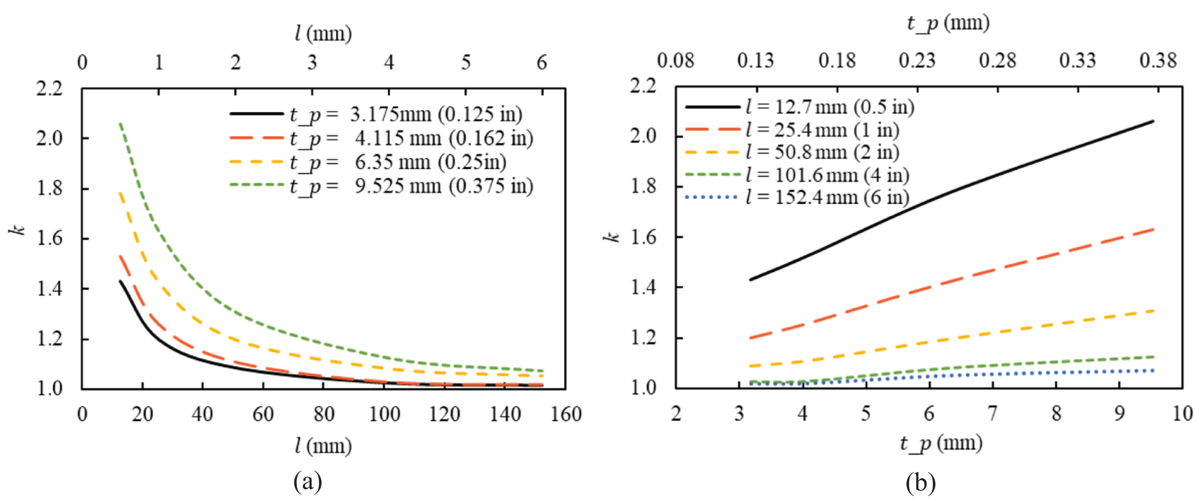


**Fig. 25.** Average stress factor against (a) crack widths with varying SIRP thickness and (b) SIRP thickness for different crack widths.

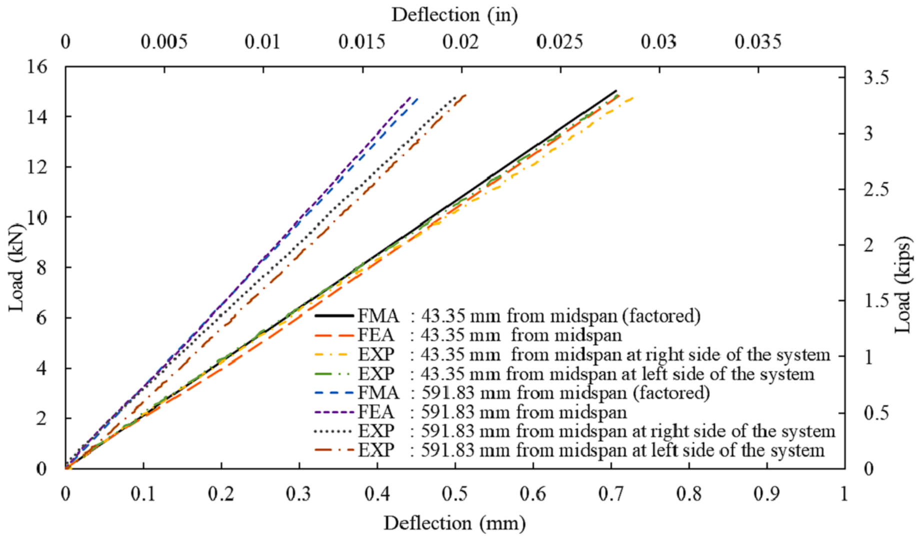


**Fig. 27.** Comparison of FMA, 3D FEA and experimental load–displacement behaviours of SIRP in host pipe with 12.7 mm opening.

prediction are approximately 1.9% and 2.2%, respectively. Furthermore, under the same loading, the highest discrepancies between the deflections predicted by the factored FMA and the laboratory experiment at the crack edge and loading point, respectively, are around 4.7% and 10.8%.

It should be noted that the developed FMA can reliably predict the load–deflection behaviour of fully bonded SIRP repair systems under lateral loading until the ultimate strain of repair material is reached. This model can be extended to account to predict the capacity of the repair system against local failure modes such as buckling as well as the influence of the combination loading cases and the effect of the unbonded length during bending. Further analyses and verification can be implemented to extend the developed FMA to predict such complex behaviour.

## 5. Conclusions

The flexural behaviour of structural internal replacement pipe (SIRP) system alone, SIRP in a continuous host pipe, and SIRP in a host pipe with narrow and wide crack widths under the effect of wheel loads located directly and moving parallel to the longitudinal axis of a pipeline have been investigated numerically in this study. The effect of the crack width of the host pipe, thickness, and material properties of the SIRP, on the bending behaviour of the composite pipe repair system, was systematically evaluated. From the results of these analyses and investigations, the following conclusions can be drawn:

- The lateral deformation of SIRP alone increases nonlinearly with the applied load and their failure mechanism is governed by local buckling of the crown.
- The lateral deformation behaviour of a continuous steel pipe system with SIRP is mostly influenced by the host pipe. The failure of the system is initiated by the yielding of the host pipe followed by local inward buckling of the SIRP. While the inclusion of the SIRP does not improve the load at yielding of the host pipe, it increases the ultimate load and maximum deflection capacity of the system by 11% and 23%, respectively.
- The lateral deformation behaviour of the repair system with a narrow circumferentially crack host pipe is governed by the host pipe while that of the system with wide cracks is governed by the SIRP systems. The strength and stiffness of the system decrease with the increase in crack width. Regardless of the crack width, the mode of failure is due to local outward buckling of the crown of SIRP between the crack edges.
- The increase in the SIRP thickness increases the flexural capacity of the system, with a nonlinear increase for the systems with a wide crack but a linear increase for the system with narrow crack widths. The thickness of the SIRP has a more substantial impact on the lateral deformation of the system with wider than narrower crack widths. The SIRP system with crack widths of 12.7 mm (0.5 in.) and 152.4 mm (6 in.) respectively require repair thicknesses of at least 9.345 mm (0.368 in.) and 13.854 mm (0.545 in.) to safely carry the design load of 178 kN (40 kips).
- The midspan deflection lowers dramatically as the elastic modulus of SIRP increases from 1 GPa (145 ksi) to 24.5 GPa (3,553 ksi). The change in E of SIRP has a greater effect on the lateral deformation of the system with wider than narrower crack widths.
- The mechanical contribution of the inner liner pipe is an important consideration in the analysis of SIRP systems because, at the same loading levels, SIRP systems in circumferentially cracked host pipes with different stiffness undergo varying levels of deformation.
- The simplified FMA can reliably predict the lateral deformation behaviour of SIRP systems in host pipes with wide circumferential cracks. The factored FMA considering the ratio of the average normal stress along the crack width from the FEA to that of the corresponding average FMA stresses can accurately predict of load-midspan deflection behaviour of the system with narrow circumferential cracks.

## Declaration of Competing Interest

The authors declare that they have no known competing financial interests or personal relationships that could have appeared to influence the work reported in this paper.

## Data availability

Data will be made available on request.

## Acknowledgement

The information, data, or work presented herein was funded in part by the Advanced Research Projects Agency-Energy (ARPA-E), US Department of Energy, under Award Number DE-AR0001327. The views and opinions of authors expressed herein do not necessarily state or reflect those of the United States Government or any agency thereof.

## References


[1] Tafsirojjaman T, Manalo A, Tien CMT, Wham BP, Salah A, Kiriella S, et al. Analysis of failure modes in pipe-in-pipe repair systems for water and gas pipelines. Eng Fail Anal 2022;140:106510.
[2] Zhang S, Zhou W. Cost-based optimal maintenance decisions for corroding natural gas pipelines based on stochastic degradation models. Eng Struct 2014;74:74–85.
[3] Ossai CI, Boswell B, Davies IJ. Pipeline failures in corrosive environments A conceptual analysis of trends and effects. Eng Fail Anal 2015;53:36–58.
[4] Sun J, Cheng YF. Assessment by finite element modeling of the interaction of multiple corrosion defects and the effect on failure pressure of corroded pipelines. Eng Struct 2018;165:278–86.
[5] Pimentel JT, et al. New procedure of automatic modeling of pipelines with realistic shaped corrosion defects. Eng Struct 2020;221:111030.
[6] Shamsuddoha Md, Islam MM, Aravinthan T, Manalo A, Lau K-T. Effectiveness of using fibre-reinforced polymer composites for underwater steel pipeline repairs. Compos Struct 2013;100:40–54.
[7] Rohem NRF, Pacheco LJ, Budhe S, Banea MD, Sampaio EM, de Barros S. Development and qualification of a new polymeric matrix laminated composite for pipe repair. Compos Struct 2016;152:737–45.
[8] Al-Abtah FG, Mahdi E, Eliyan FF. The use of fiber reinforced polymeric composites in pipelines: A review. Compos Struct 2021;276:114595.
[9] Yang H-N, Chen J-H, Chiu H-J, Kao T-J, Tsai H-Y, Chen J-R. Confined vapor explosion in Kaohsiung City – A detailed analysis of the tragedy in the harbor city. J Loss Prev Process Ind 2016;41:107–20.
[10] Witek M, Batura A, Orynyak I, Borodii M. An integrated risk assessment of onshore gas transmission pipelines based on defect population. Eng Struct 2018;173:150–65.
[11] Biezma MV, et al. Most fatal oil & gas pipeline accidents through history: A lessons learned approach. Eng Fail Anal 2020;110.
[12] Chin WS, Lee DG. Development of the trenchless rehabilitation process for underground pipes based on RTM. Compos Struct 2005;68(3):267–83.
[13] Karbhari VM. Rehabilitation of Pipelines Using Fiber-reinforced Polymer (FRP) Composites. 2014. Cambridge, United Kingdom: Elsevier Science; 2015.
[14] Pesinis K, Tee KF. Bayesian analysis of small probability incidents for corroding energy pipelines. Eng Struct 2018;165:264–77.
[15] Li Z, Tang F, Chen Y, Zou X. Stability of the pipe-liner system with a grouting void surrounded by the saturated soil. Eng Struct 2019;196:109284.
[16] Selvakumar A, et al. State of technology for rehabilitation of water distribution system. Edison, NJ, USA: US Environmental Protection Agency (EPA); 2013.
[17] Rahmaninezhad SM, et al. Field evaluation of performance of corroded corrugated steel pipe before and after sliplining rehabilitation. Tunn Undergr Space Technol 2020;102:103442.
[18] Wu Y, Kang C, Nojumi MM, Bayat A, Bontus G. Current water main rehabilitation practice using trenchless technology. Water Pract Technol 2021;16(3):707–23.
[19] Jung YJ, Sinha SK. Evaluation of trenchless technology methods for municipal infrastructure system. J Infrastruct Syst 2007;13(2):144–56.
[20] Yu HN, Kim SS, Hwang IU, Lee DG. Application of natural fiber reinforced composites to trenchless rehabilitation of underground pipes. Compos Struct 2008;86(1-3):285–90.
[21] Czél G, Czigány T. Finite element method assisted stiffness design procedure for non-circular profile composite wastewater pipe linings. Compos Struct 2014;112:78–84.
[22] Lu H, Behbahani S, Azimi M, Matthews JC, Han S, Iseley T. Trenchless construction technologies for oil and gas pipelines: State-of-the-art review. J Constr Eng Manag 2020;146(6).
[23] Jeon S-S, O'Rourke TD, Neravali AN. Repetitive loading effects on cast iron pipelines with cast-in-place pipe lining system. J Transport Eng-ASCE 2004;130:692–705.
[24] Argyrou C, O'Rourke TD, Stewart HE, Wham BP. Large-scale fault rupture tests on pipelines reinforced with cured-in-place linings. J Geotech Geoenviron Eng 2019;145(3).
[25] Vasseghi A, Haghshenas E, Soroushian A, Rakhshandeh M. Failure analysis of a natural gas pipeline subjected to landslide. Eng Fail Anal 2021;119:105009.
[26] Vazouras P, Karamanos SA, Dakoulas PC. Mechanical behavior of buried steel pipes crossing active strike-slip faults. Soil Dyn Earthq Eng 2012;41:164–80.
[27] Liu Wu, Guo Q, Qiao C, Hou W. Strain design method of buried pipeline crossing fault. Eng Fail Anal 2019;105:659–71.
[28] Melissianos VE, Vamvatsikos D, Gantes CJ. Performance-based assessment of protection measures for buried pipes at strike-slip fault crossings. Soil Dyn Earthq Eng 2017;101:1–11.
[29] Guo B, et al. Offshore Pipelines. 1 ed. Burlington, MA: Elsevier; 2005.
[30] Costa Mattos HSd, Reis JML, Paim LM, Silva MLd, Lopes Junior R, Perrut VA. Failure analysis of corroded pipelines reinforced with composite repair systems. Eng Fail Anal 2016;59:223–36.
[31] Budhe S, Banea MD, de Barros S. Composite repair system for corroded metallic pipelines: an overview of recent developments and modelling. J Mar Sci Technol 2020;25(4):1308–23.
[32] Bokaian A. Thermal expansion of pipe-in-pipe systems. Mar Struct 2004;17(6):475–500.
[33] Zhong Z, Wang S, Zhao Mi, Du X, Li L. Performance of ductile iron push-on joints rehabilitated with CIPP liner under repetitive and seismic loadings. Soil Dyn Earthq Eng 2018;115:776–86.
[34] Ng PCF. Behaviour of buried pipelines subjected to external loading. In: Department of civil and structural engineering. University of Sheffield; 1994. p. 339.
[35] Stewart HE, Netravali AN, O'Rourke TD. Performance testing of field-aged cured-in-place liners (CIPL) for cast iron piping. School of Civil and Environmental Engineering, Cornell University; 2015. p. 1–128.
[36] Makar JM, Desnoyers R, McDonald SE. Failure modes and mechanisms in gray cast iron pipe. ttawa, Ontario, Canada: Institute for Research in Construction, National Research Council Canada; 2001. p. 1–10.
[37] Farag MH, Mahdi E. New approach of pipelines joining using fiber reinforced plastics composites. Compos Struct 2019;228:111341.
[38] Mahdi E, Eltai EO. Development of cost-effective composite repair system for oil/gas pipelines. Compos Struct 2018;202:802–6.
[39] Sirimanna CS, Banerjee S, Karunasena W, Manalo AC, McGarva L. Analysis of retrofitted corroded steel pipes using internally bonded FRP composite repair systems. Aust J Struct Eng 2015;16(3):187–98.
[40] Lim KS, Azraai SNA, Yahaya N, Md Noor N, Zardasti L, Kim J-H. Behaviour of steel pipelines with composite repairs analysed using experimental and numerical approaches. Thin-Walled Struct 2019;139:321–33.
[41] Yeleswarapu S, Chandra Khan V, P. NK, Gurusamy B, Pandit MK. Performance assessment of polymeric composite wrap to repair damaged pipelines exposed under accelerated environment conditions. J Pipeline Syst Eng Pract 2021;12(3).
[42] Saeed N, Kang W-H, Samali B. Composite overwrap repair of pipelines-reliability based design framework. Structures 2022;40:448–59.
[43] Sever VF, Ehsani M. *Designing an Economical FRP System for Pipeline Rehabilitation*. In: *Pipelines 2019*. 2019.
[44] Fan T, Liu Z, Li M, Zhao Y, Zuo Z, Guo R. Development of cost-effective repair system for locally damaged long-distance oil pipelines. Constr Build Mater 2022;333:127342.
[45] Chen J, et al. Finite element analysis of composite repair for damaged steel pipeline. Coatings 2021;11:301.
[46] Allouche EN, et al. Experimental Examination of selected limit states of structural liners at locations of ring fracture. In: *Pipelines Conference 2012*. 2012. p. 783-794.
[47] Shou KJ, Chen BC. Numerical analysis of the mechanical behaviors of pressurized underground pipelines rehabilitated by cured-in-place-pipe method. Tunn Undergr Space Technol 2018;71:544–54.
[48] Yang K, Xue B, Fang H, Du X, Li B, Chen J. Mechanical sensitivity analysis of pipe-liner composite structure under multi-field coupling. Structures 2021;29:484–93.
[49] Sousa R, Sousa H, Guedes JPM. Diagonal compressive strength of masonry sample" experimental and numerical approach. Mater Struct 2013;46:765–86.
[50] Ansys, Finite Element Analysis (FEA). Software for Structuaral Engineering. ANSYS, Inc.; 2021.
[51] Preedawiphat P, Mahayotsanun N, Sa-ngoen K, Noipitak M, Tuengsook P, Sucharitpwatskul S, et al. Mechanical investigations of ASTM A36 welded steels with stainless steel cladding. Coatings 2020;10(9):844.
[52] ASTM, Standard Test Method for Tensile Properties of Plastics. In: ASTM D638-14. ASTM International; 2015. p. 1-17.
[53] Gereber WS. In: IngVer ZBA (eds.) Calculation of the allowable stresses in iron structures. Vol. 6. P. 101-110. 1874.
[54] Manalo AC, Aravinthan T, Karunasena W, Islam MM. Flexural behaviour of structural fibre composite sandwich beams in flatwise and edgewise positions. Compos Struct 2010;92(4):984–95.
[55] MATLAB. MATLAB version 9.9.0.1524771 (R2020b) Update 2. The Mathworks, Inc.: Natick, Massachusetts; 2020.
[56] Manalo A. Behaviour of fibre composite sandwich structures: A case study on railway sleeper application. In: Centre of excellence in engineered fibre composites, faculty of engineering and surveying. University of Southern Queensland; 2011. p. 305.